Algorithm Theoretical Basis Document (ATBD) Bremen Optimal Estimation DOAS (BESD v01.00.01)

Version 1

ESA Climate Change Initiative (CCI)
for the Essential Climate Variable (ECV)

Greenhouse Gases (GHG)

Prepared by:

M. Reuter, H. Bovensmann, M. Buchwitz, J. P. Burrows, J. Heymann,
O. Schneising, H. Schnisa, V. Velazco

Institute of Environmental Physics (IUP)
University of Bremen, FB1
PO Box 33 04 40
D-28334 Bremen
Germany

Contents

1 Introduction

This algorithm theoretical basis document (ATBD) describes in detail the Bremen optimal estimation DOAS algorithm BESD (with the algorithm version number v01.00.01). In large parts, this document is compiled from text and figures of the publications of Reuter et al. (2010) and Reuter et al. (2011).

Although CO_2 is the dominant anthropogenic greenhouse gas, there are still large uncertainties of its natural global sources and sinks (Stephens et al., 2007). The theoretical studies of Rayner and O'Brien (2001) and Houweling et al. (2004) showed that satellite measurements of CO_2 have the potential to significantly reduce surface flux uncertainties if a precision of about 1% for regional averages and monthly means can be achieved. However, Miller et al. (2007) and Chevallier et al. (2007) found that undetected biases of a few tenths of a part per million on regional scales can limit surface flux inverse modeling.

Presently, there are only two satellite instruments orbiting the Earth which enable the retrieval of the column-average dry-air mole fraction of atmospheric carbon dioxide (XCO_2) with significant sensitivity in the boundary layer where the largest signals of sources and sinks occur. These are SCIAMACHY (Scanning Imaging Absorption Spectrometer for Atmospheric CHartographY) (Burrows et al., 1995; Bovensmann et al., 1999) aboard ENVISAT (ENVIronmental SATellite), which was launched in 2002, and TANSO (Thermal And Near infrared Sensor for carbon Observation) (Yokota et al., 2004) aboard GOSAT (Greenhouse gases Observing SATellite), which was launched in 2009. Both instruments measure near- and short-wave-infrared (in the following referred to as NIR) reflected solar radiation in absorption bands at around 0.76, 1.6, and 2.0 μm. OCO (Orbiting Carbon Observatory) (Crisp et al., 2004) was another satellite designed to observe atmospheric carbon dioxide in the same spectral regions as TANSO and SCIAMACHY. Unfortunately, the satellite was lost shortly after lift-off on 24 February 2009.

In contrast to TANSO and OCO, SCIAMACHY was not specifically designed for the retrieval of XCO_2. As a result of SCIAMACHY's coarser spatial and spectral resolution, the achievable accuracy is expected to be lower. Nevertheless, within the years 2002 to 2009 SCIAMACHY was the only satellite instrument measuring XCO_2 with significant sensitivity in the boundary layer. Therefore, the retrieval of XCO_2 from SCIAMACHY with realistic error estimates is crucial to start a consistent long-term time series of XCO_2 observations from space.

Generally, scattering related errors remain a major source of uncertainty for SCIAMACHY XCO_2 retrievals and easily exceed the precision and accuracy estimates for clear sky conditions. This is supported by the following two examples:

Mineral dust aerosols may introduce retrieval errors of 10% (Houweling et al., 2005). Undetected cirrus clouds with a cloud optical thickness (COT) below 0.1 can result in retrieval errors of about 8% (Aben et al., 2007; Schneising et al., 2008).

For the high spectral resolution instruments TANSO and OCO, algorithms have been developed that correct for scattering effects (Kuang et al., 2002; Bril et al., 2007; Connor et al., 2008; Butz et al., 2009). BESD aims to significantly reduce scattering related errors of SCIAMACHY retrieved XCO_2. It uses SCIAMACHY nadir data at 0.76 and 1.6 μm and explicitly considers scattering by an (optically thin) ice cloud layer and aerosols assuming a default profile.

2 Algorithm Overview

BESD is designed to analyze near-infrared nadir measurements of the SCIAMACHY instrument in the CO_2 absorption band at 1580 nm and in the O_2-A absorption band at around 760 nm. The algorithm is a so called full physics algorithm which explicitly accounts for scattering in an optically thin cirrus cloud layer and at aerosols of a default profile. The scattering information is mainly obtained from the O_2-A band and a merged fit windows approach enables the transfer of information between the O_2-A and the CO_2 band. This technique makes BESD relatively insensitive in respect to unknown scattering properties. Systematic errors due to scattering are most times below 4 ppm. Via the optimal estimation technique, the algorithm is able to account for a priori information to further constrain the inversion.

2.1 Physical Basis

BESD retrieves several independent parameters from SCIAMACHY measurements in the spectral region dominated by CO_2 absorption from 1558 nm to 1594 nm (in the following referred to as the "CO_2 fit window") and also from measurements in the spectral region of the O_2-A band from 755 nm to 775 nm nm (in the following referred to as the "O_2 fit window"). The list of retrieval parameters such as CO_2 mixing ratio, surface pressure, cloud top height, albedo, etc, ... defines the state vector.

Each of these parameters influences the spectrum of reflected solar radiation measured at the satellite instrument. The partial derivatives of the measured radiation with respect to a parameter is called the weighting function (or Jacobian) of this parameter. Of course, it is only possible to retrieve those

parameters having a unique weighting function, sufficiently different from all other weighting functions in terms of the instrument's accuracy. Very similar weighting functions can result in ambiguities of the retrieved corresponding parameters.

Fig. 1 shows for exemplary atmospheric conditions with moderate aerosol load and one thin ice cloud layer the weighting functions of three different scattering related parameters under a typical observation geometry in SCIAMACHY's spectral resolution. Additionally, the figure shows the XCO_2 weighting function which gives the change of radiation when columnar increasing the CO_2 concentration by 1 ppm. For this example, the magnitude of its spectral signature is comparable to a change of the cloud top height (CTH) by 1 km, the cloud water/ice path (CWP) by 0.2 g/m^2, or to a change of the aerosol load by 100%. It is immediately noticeable that there are high correlations between the curves. Especially between the aerosol profile scaling (APS) and the cloud water/ice path weighting function as well as between the cloud top height and the XCO_2 weighting function.

XCO_2 changes of 1 ppm are approximately the detection limit due to SCIAMACHY's signal to noise (SNR) characteristics. This means, with SCIAMACHY it is actually not possible to discriminate XCO_2 values of a few ppm from changes of the given scattering parameters. For example, decreasing the cloud top height from 14 km to 10 km spectrally changes the radiation in (nearly) the same way as increasing XCO_2 by 4 ppm does. Most likely, it is not possible to retrieve scattering parameters simultaneously with the number of CO_2 molecules, i.e., uncertainties of the scattering parameters will always result in uncertainties of the retrieved CO_2 molecules when solely analyzing measurements from the CO_2 fit window.

Analog to Fig. 1, Fig. 2 shows for identical atmospheric conditions the weighting functions of the same scattering parameters but for the O_2 fit window. Additionally, it shows the weighting function in respect to surface pressure p_s which can be used to derive the total number of air molecules within the atmospheric column by applying the hydrostatic assumption. The similarities between the weighting functions are less pronounced in this fit window. This applies especially when comparing the surface pressure weighting function to the weighting functions of the given scattering parameters. This originates by much stronger absorption lines in this fit window. As width and depth of absorption lines depend on the ambient pressure, saturation effects differ much stronger with height within this spectral region. Additionally, SCIAMACHY's resolution resolves the spectral structures of the gaseous absorption better within this fit window. Nevertheless, there are still similarities that are not negligible e.g.

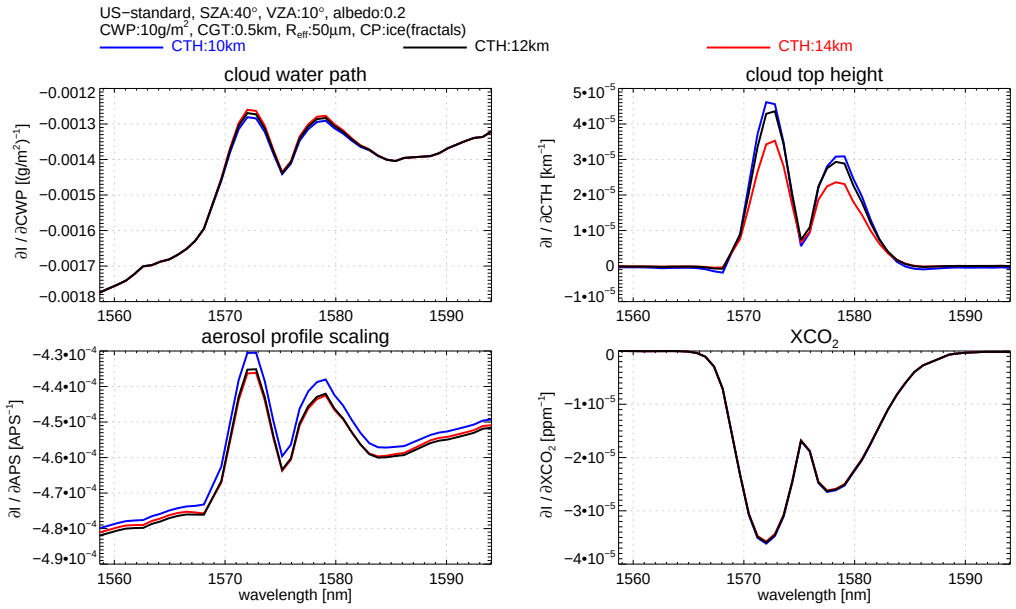

Figure 1: Weighting functions in the CO_2 fit window for three cloud scenarios based on a US-standard atmosphere including an optically thin ice cloud with a cloud top height of 10 km (**blue**), 12 km (**black**), and 14 km (**red**): cloud water/ice path (**top/left**), cloud top height (**top/right**), scaling of the aerosol profile (**bottom/left**), and XCO_2 (**bottom/right**). The weighting functions are calculated with the SCIATRAN 3.2 radiative transfer code and are convolved with SCIAMACHY's slit function.

between the cloud top height and aerosol profile scaling weighting function. Differences of 1 hPa are in the order of the detection limit according to SCIAMACHY's SNR characteristics. Therefore, it can be expected that independent information on the given scattering parameters can be extracted from this fit window simultaneously with information about the surface pressure.

The large differences of the three illustrated cloud top height weighting functions show that the radiative transfer can become non-linear in respect to this parameter. Additionally, the spectral similarity of the CTH and the CWP weighting function strongly depend on the scenario (large differences for the cloud at 12 km, minor differences for the cloud at 10 km). This means, depending on the individual scene, ambiguities may be more or less pronounced. In this context, also the selected surface albedo has strong influence.

Section 3 will describe, how the information on scattering parameters, which can be derived from the O_2 fit window, can be transported to the CO_2 fit

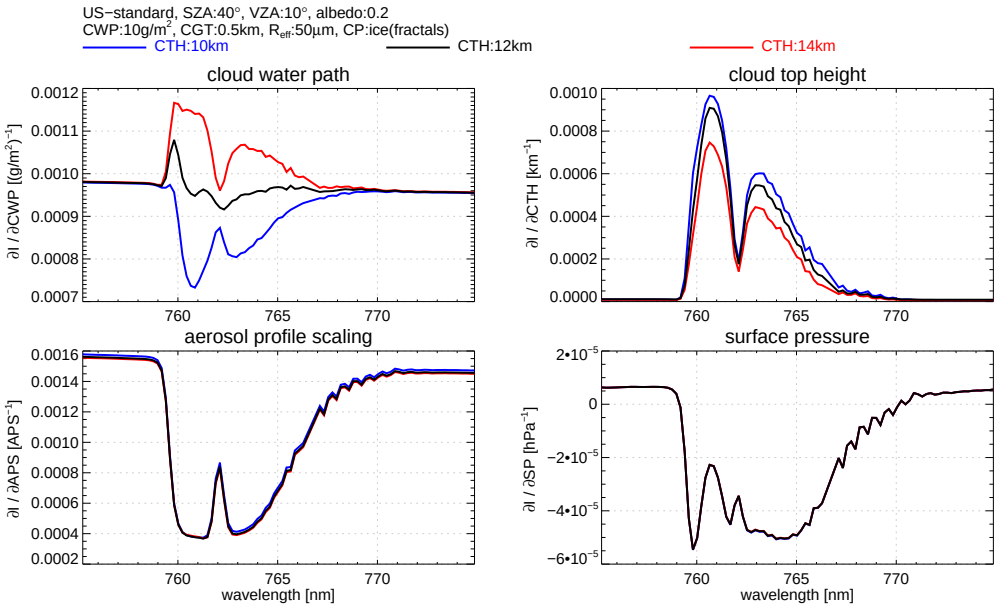

Figure 2: Weighting functions in the O_2 fit window for three cloud scenarios based on a US-standard atmosphere including an optically thin ice cloud with a cloud top height of 10 km (**blue**), 12 km (**black**), and 14 km (**red**): cloud water/ice path (**top/left**), cloud top height (**top/right**), scaling of the aerosol profile (**bottom/left**), and surface pressure (**bottom/right**). The weighting functions are calculated with the SCIATRAN 3.2 radiative transfer code and are convolved with SCIAMACHY's slit function.

window.

2.2 Input Data

SCIAMACHY nadir and corresponding sun spectra of 7.xx are the main input for the XCO_2 retrieval algorithm BESD. The SCIAMACHY data is calibrated with ESA's SciaL1C calibration and extraction tool for SCIAMACHY level 1b data by applying all implemented calibration procedures. This includes also the usage of M-factors, which correct for instrumental degradation.

Other inputs for BESD are ECMWF (European Centre for Medium-Range Weather Forecasts) re-analysis profiles of temperature, pressure and humidity. A digital elevation model is used to calculate the first guess of the surface pressure considering sub-pixel variations of the surface height. All other inputs are constant in space and time. This applies especially to the a priori CO_2

profile.

Even though BESD is designed to minimize errors as a result of scattering in the light path, undetected clouds are still an important possible source of error. Therefore, strict cloud filtering is still necessary. For this purpose, the MERIS (MEdium Resolution Imaging Spectrometer) cloud detection algorithm is used which is part of ESA's Basic ENVISAT Toolbox for AATSR and MERIS (BEAM, *http://www.brockmann-consult.de/beam*). The MERIS cloud mask with approximately 1×1 km^2 resolution gives important information about SCIAMACHY's sub-pixel cloud coverage. Only those SCIAMACHY pixels which are 100% cloud free within the pixel and within a surrounding of 40 km are considered.

Likewise, the SCIAMACHY absorbing aerosol index (AAI) (**?**) with a threshold of 0.0 is utilized to filter aerosol contaminated scenes. Additionally, only fully land covered scenes with a surface roughness less then 0.5 km and with a solar zenith angle less then 70^o are considered.

2.3 Output Data

Only those measurements which fulfill all quality criteria are stored in orbitwise result files in NCDF file format. Their file names consist of (an abbreviation of) the retrieved gas (CO2), the instrument (SCI), the algorithm (BESD_vXX.XX.XX, where XX.XX.XX is a version number), and the date (YYYYMMDD), e.g. CO2_SCI_BESD_v01.00.01_20100321.nc

The result files contain all the information required for surface flux inverse modeling such as retrieved XCO_2 values for individual ground pixels, their errors, corresponding averaging kernels, used a priori profiles, etc. In order to provide this and allow comparisons with other remote or in-situ measurements as well as models, the result files contain the parameters found in Tab. 1.

In the future, the result files will give also information about error reduction, information content, degree of freedom, first guess, a priori, and retrieval result of each state vector element as well as the error covariance matrices of the a priori, a posteriori, and the measurement, the gain and averaging kernel matrices, the measurement vector and its spectral fit.

3 Mathematical Algorithm Description

BESD uses an optimal estimation based inversion technique to find the most probable atmospheric state given a SCIAMACHY measurement and some prior knowledge. Nearly all mathematical expressions given in this ATBD as well as

Table 1: List of output parameters contained in orbit-wise BESD result files in NCDF file format. Dimensions are defined as number of pixels per orbit (n) and number of pressure levels (m).

Parameter	Type	Dimension	Unit	Description
instrument	String	1	-	SCIAMACHY
l2_processing_institute	String	1	-	IUP
l2_processor_version	String	1	-	Processor Version Number
l1b_input_filename	String	1	-	L1B Filename
solar_zenith_angle	Float	n	Degrees	Solar Zenith Angle (0^o=zenith)
viewing_zenith_angle	Float	n	Degrees	Viewing Zenith Angle (0^o=nadir)
azimuth_difference	Float	n	Degrees	Azimuth Difference
time	Double	n	Seconds	Seconds since 01.01.1970 00:00 UTC
longitude_centre	Float	n	Degrees	Longitude of pixel centre
latitude_centre	Float	n	Degrees	Latitude of pixel centre
longitude_corners	Float	n×4	Degrees	Longitude of pixel corners
latitude_corners	Float	n×4	Degrees	Latitude of pixel corners
surface_elevation	Float	n	km	Mean surface elevation of pixel
pressure_levels	Float	n×m	hPa	Retrieval pressure levels
column_averaging_kernel	Float	n×m	-	Normalized Column Averaging Kernel Profile
chi2	Float	n	-	Chi-Square of fit residual
rms	Float	n	-	Relative RMS of fit residual
xco2	Float	n	ppm	Retrieved XCO_2
xco2_uncertainty	Float	n	ppm	Uncertainty in Retrieved XCO_2
xco2_apriori	Float	n	ppm	A priori XCO_2
vmr_profile_co2	Float	n×m	ppm	Retrieved CO_2 profile
vmr_profile_co2_uncertainty	Float	n×m	ppm	Uncertainty in Retrieved CO_2 profile
vmr_profile_co2_apriori	Float	n×m	ppm	A priori CO_2 profile

their derivation and notation can be found in the text book of Rodgers (2000). A list of used symbols is given by Tab. 2.

The forward model **F** is a vector function which calculates for a given (atmospheric) state simulated measurements i.e. simulated SCIAMACHY spectra. The input for the forward model are the state vector **x** and the parameter vector **b**. The state vector consists of all unknown variables that shall be retrieved from the measurement (e.g. CO_2). Parameters which are assumed to be exactly known but affecting the radiative transfer (e.g. viewing geometry) are the elements of the parameter vector. The entire list of state vector elements is given in the first column of Tab. 4. The measurement vector **y** consists of SCIAMACHY sun-normalized radiances of two merged fit windows concatenating the measurements in the CO_2 and O_2 fit window. The difference of measurement and corresponding simulation by the forward model is given by the error vector ε comprising inaccuracies of the instrument and of the forward model:

$$\mathbf{y} = \mathbf{F}(\mathbf{x}, \mathbf{b}) + \varepsilon \tag{1}$$

According to Eq. 5.3 of Rodgers (2000), BESD aims to find the state vector $\mathbf{x}$ which minimizes the cost function χ^2:

$$\begin{aligned}\chi^2 &= (\mathbf{y}-\mathbf{F}(\mathbf{x},\mathbf{b}))^T\mathbf{S}_\epsilon^{-1}(\mathbf{y}-\mathbf{F}(\mathbf{x},\mathbf{b})) \\ &\quad +(\mathbf{x}-\mathbf{x}_a)^T\mathbf{S}_a^{-1}(\mathbf{x}-\mathbf{x}_a) \end{aligned} \tag{2}$$

Here, $\mathbf{S}_\epsilon$ is the error covariance matrix corresponding to the measurement vector, $\mathbf{x}_a$ is the a priori state vector which holds the prior knowledge about the state vector elements and $\mathbf{S}_a$ is the corresponding a priori error covariance matrix which specifies the uncertainties of the a priori state vector elements as well as their cross correlations.

Even though the number of state vector elements (26) is smaller than the number of measurement vector elements (134), the inversion problem is generally under-determined. The weighting functions of some state vector elements show quite large correlations under certain conditions. This especially applies to the weighting functions corresponding to the ten-layered CO_2 profile but also to some of the weighting functions shown in Fig. 1 and Fig. 2. For this reason BESD uses a priori knowledge further constraining the problem and making it well-posed. However, for most of the state vector elements the used a priori knowledge gives only a weak constraint and is therefore not dominating the retrieval results. Furthermore, only static a priori knowledge of XCO_2 is used.

According to Eq. 5.36 of Rodgers (2000), BESD uses a Levenberg-Marquardt method to iteratively find the state vector $\hat{\mathbf{x}}$ which minimizes the cost function.

$$\mathbf{x}_{i+1} = \mathbf{x}_i + \hat{\mathbf{S}}[\mathbf{K}_i^T\mathbf{S}_\epsilon^{-1}(\mathbf{y}-\mathbf{F}(\mathbf{x}_i,\mathbf{b})) - \mathbf{S}_a^{-1}(\mathbf{x}_i-\mathbf{x}_a)] \tag{3}$$

$$\hat{\mathbf{S}} = (\mathbf{K}_i^T\mathbf{S}_\epsilon^{-1}\mathbf{K}_i + (1+\gamma)\mathbf{S}_a^{-1})^{-1} \tag{4}$$

Within this equation, $\mathbf{K}$ is the Jacobian or weighting function matrix consisting of the derivatives of the forward model in respect to the state vector elements $\mathbf{K} = \partial\mathbf{F}(\mathbf{x},\mathbf{b}))/\partial\mathbf{x}$. In the case of convergence, $\mathbf{x}_{i+1}$ is the most probable solution given the measurement and the prior knowledge and is then denoted as maximum a posteriori solution $\hat{\mathbf{x}}$ of the inverse problem. $\hat{\mathbf{S}}$ is the corresponding covariance matrix consisting of the variances of the retried state vector elements and their correlations.

The damping factor γ adjusts the step size of the iteration in a way which ensures that each (successful) step further minimizes the cost function. This requires the ratio R of the change of the cost function computed properly to that computed with the linear approximation of the forward model:

$$R = ({\chi_i}^2 - {\chi_{i+1}}^2)/({\chi_i}^2 - {\chi'_{i+1}}^2) \tag{5}$$

$$\begin{aligned} {\chi'_{i+1}}^2 &= (\mathbf{y}-\mathbf{F}'(\mathbf{x}_{i+1},\mathbf{b}))^T\mathbf{S}_\epsilon^{-1}(\mathbf{y}-\mathbf{F}'(\mathbf{x}_{i+1},\mathbf{b})) \\ &\quad +(\mathbf{x}_{i+1}-\mathbf{x}_a)^T\mathbf{S}_a^{-1}(\mathbf{x}_{i+1}-\mathbf{x}_a) \qquad (6) \\ \mathbf{F}'(\mathbf{x}_{i+1},\mathbf{b}) &= \mathbf{F}(\mathbf{x}_i,\mathbf{b})+\mathbf{K}_i(\mathbf{x}_{i+1}-\mathbf{x}_i) \qquad (7) \end{aligned}$$

R is unity if the forward model can perfectly be described by its linear approximation. In the case χ^2 has increased rather than decreased, R becomes negative and the iteration step is rejected. The following strategy is used to find a value of γ which restricts $\mathbf{x}_{i+1}$ to lie within the linear range i.e. the so called "trust region" of $\mathbf{F}(\mathbf{x}_i,\mathbf{b})$: if $R > 0.75$ than reduce γ by a factor of 2, if $R < 0.25$ than enhance γ by a factor of 2, otherwise make no changes.

The iteration starts with $\gamma = 1$ and the first guess state vector $\mathbf{x}_0$. Often, $\mathbf{x}_0$ is set to $\mathbf{x}_a$, even though this is mathematically not mandatory and also not done here for some state vector elements. Referring to Eq. 5.29 of Rodgers (2000), BESD tests for convergence by relating the changes of the state vector to the error covariance $\hat{\mathbf{S}}$ after each iteration. If the value of $(\mathbf{x}_i-\mathbf{x}_{i+1})^T\hat{\mathbf{S}}^{-1}(\mathbf{x}_i-\mathbf{x}_{i+1})$ falls below the number of state vector elements (26), convergence is achieved and the iteration is stopped. As it is theoretically possible that convergence is never achieved, iteration also stops after seven unsuccessful steps. However, typically, the convergence criterion is fulfilled after about five iterations.

Subsequently, some terms are used also given by Rodgers (2000) to compute the gain matrix $\mathbf{G}$ (Eq. 2.45), the averaging kernel matrix $\mathbf{A}$ (Eq. 3.10), the degree of freedom for signal d_s (Eq. 2.80), and the information content H (Eq. 2.80). The gain matrix corresponds to the sensitivity of the retrieval to the measurement and is given by:

$$\mathbf{G} = (\mathbf{K}^T\mathbf{S}_\epsilon^{-1}\mathbf{K}+\mathbf{S}_a^{-1})\mathbf{K}^T\mathbf{S}_\epsilon^{-1} \qquad (8)$$

Having the gain matrix, the averaging kernel matrix can be compute which is the sensitivity of the retrieval to the true state:

$$\mathbf{A} = \mathbf{GK} \qquad (9)$$

The degree of freedom for signal corresponds to the number of independent quantities that can be derived from the measurement and is given by:

$$d_s = \mathrm{tr}(\mathbf{A}) \qquad (10)$$

The information content gives the number of different atmospheric states that can be distinguished in bits:

$$H = -\frac{1}{2}\ln(|\mathbf{I}-\mathbf{A}|) \qquad (11)$$

The degree of freedom as well as the information content can be calculated for arbitrary sub sets of state vector elements by taking only corresponding elements of the averaging kernel matrix into account. Comparing the variances of the retrieved state vector elements with the corresponding a priori variances, the uncertainty reduction $\mathbf{r}_\sigma$ of the j^{th} state vector element is defined by:

$$\mathbf{r}_{\sigma j} = 1 - \sqrt{\hat{\mathbf{S}}_{j,j}/\mathbf{S}_{aj,j}} \tag{12}$$

Note: using merged fit windows instead of performing the retrieval in two separate fit windows has two main advantages when retrieving state vector elements which have sensitivities in both fit windows. 1) These elements are better constraint because simultaneous fitting implicitly utilizes the knowledge that the retrieved quantity (e.g. the atmospheric temperature) must be identical in both fit windows. 2) If there are state vector elements with strong ambiguities in one fit windows (e.g. surface pressure and scattering parameters in the CO_2 fit window), the information come mainly from the fit window with less ambiguities. Merging the fit windows makes this information available in both fit windows.

3.1 Forward Model

As forward model, BESD makes use of the SCIATRAN 3.2 radiative transfer code (Rozanov et al., 2005) in discrete ordinate mode. The correlated-k approach of Buchwitz et al. (2000) is used to increase the computational efficiency. As final part of the forward calculation, the resulting spectra are convolved with a SCIAMACHY like Gaussian slit function and applying the dead/bad pixel mask also used for WFM-DOAS 2.1 with additionally masked out all spectral pixels of channel 6+. Spectral line parameters are taken from the HITRAN 2008 (Rothman et al., 2009) database.

The radiative transfer calculations are performed on up to 60 model levels, even though the state vector includes only a ten-layered CO_2 mixing ratio profile. This profile is expanded to the model levels before each forward calculation. In the case of liquid water droplets, phase function, extinction, and scattering coefficient of cloud particles are calculated with Mie's theory assuming gamma particle size distributions.

In the case of ice crystals, corresponding calculations are performed with a Monte Carlo code, assuming an ensemble of randomly aligned fractal or hexagonal particles. The volume scattering function is the product of phase function and scattering coefficient. Fig. 3 illustrates the volume scattering functions of all cloud particles analyzed in Sec. 4.

Table 2: List of used symbols and corresponding dimensions and short descriptions.

Symbol	Dimension	Description
$\mathbf{A}$	$n \times n$	Averaging kernel matrix
$\mathbf{b}$	$n_b \times 1$	Parameter vector
d_l	1	Degree of non-linearity
d_s	1	Degree of freedom for signal
ε	$m \times 1$	Measurement and forward model error
$\mathbf{F}$	$m \times 1$	Forward model
$\mathbf{G}$	$n \times m$	Gain matrix
$\mathbf{K}$	$m \times n$	Weighting function matrix
H	1	Information content in bits
m	1	Size of measurement vector ($= 134$)
n	1	Size of state vector ($= 26$)
n_b	1	Size of parameter vector
n_{CO_2}	1	CO_2profile layers ($= 10$)
p_s	1	Surface pressure
$\mathbf{r}_\sigma$	$n \times 1$	Uncertainty reduction
$\hat{\mathbf{S}}$	$n \times n$	Covariance matrix of retrieved state
$\mathbf{S}_a$	$n \times n$	A priori covariance matrix
$\mathbf{S}_\epsilon$	$m \times m$	Measurement error covariance matrix
$\mathbf{w}$	$n \times 1$	Layer weighting vector
$\mathbf{x}$	$n \times 1$	State vector
$\mathbf{x}_0$	$n \times 1$	First guess state vector
$\mathbf{x}_a$	$n \times 1$	a priori state vector
$\mathbf{x}_t$	$n \times 1$	True state vector
$\hat{\mathbf{x}}$	$n \times 1$	Retrieved state vector
χ^2	1	Cost function (Eq. 2)
$\mathbf{y}$	$m \times 1$	Measurement vector

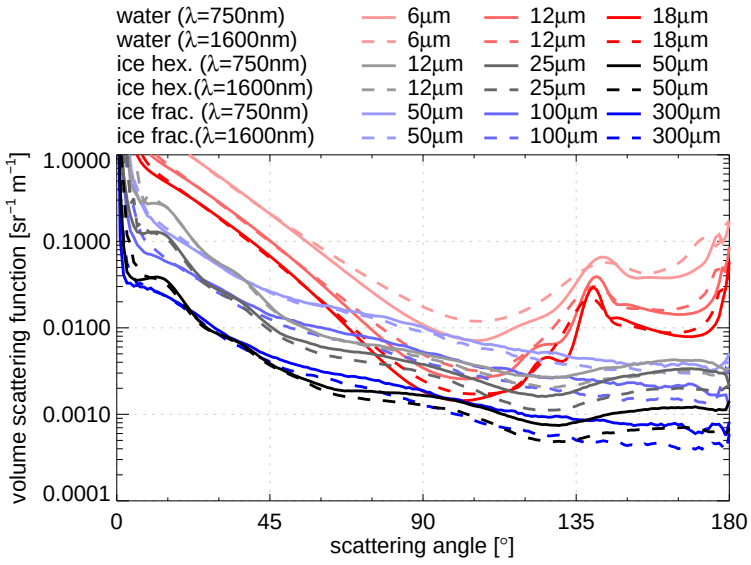

Figure 3: Volume scattering functions of all cloud particles analyzed in Sec. 4. The dominant forward peaks is cut in this clipping.

3.2 State Vector

All retrieval results shown in this ATBD are valid for a state vector consisting of 26 elements listed in the first column of Tab. 4. Corresponding weighting functions calculated for exemplary atmospheric conditions are illustrated in Fig. 4. The a priori uncertainties have been chosen so that they sufficiently constrain the inversion by defining a well-posed problem without dominating the retrieval results.

3.2.1 Wavelength Shift, Slit Function FWHM

The state vector accounts for fitting a wavelength shift and the full width half maximum (FWHM) of a Gaussian shaped instrument's slit function separately in the O_2 and CO_2 fit window. This means, the corresponding weighting functions are identical zero within the O_2 or in the CO_2 fit window, respectively.

3.2.2 Albedo

BESD assumes a Lambertian surface with an albedo with smooth spectral progression which can be expressed by a 2^{nd} order polynomial separately within

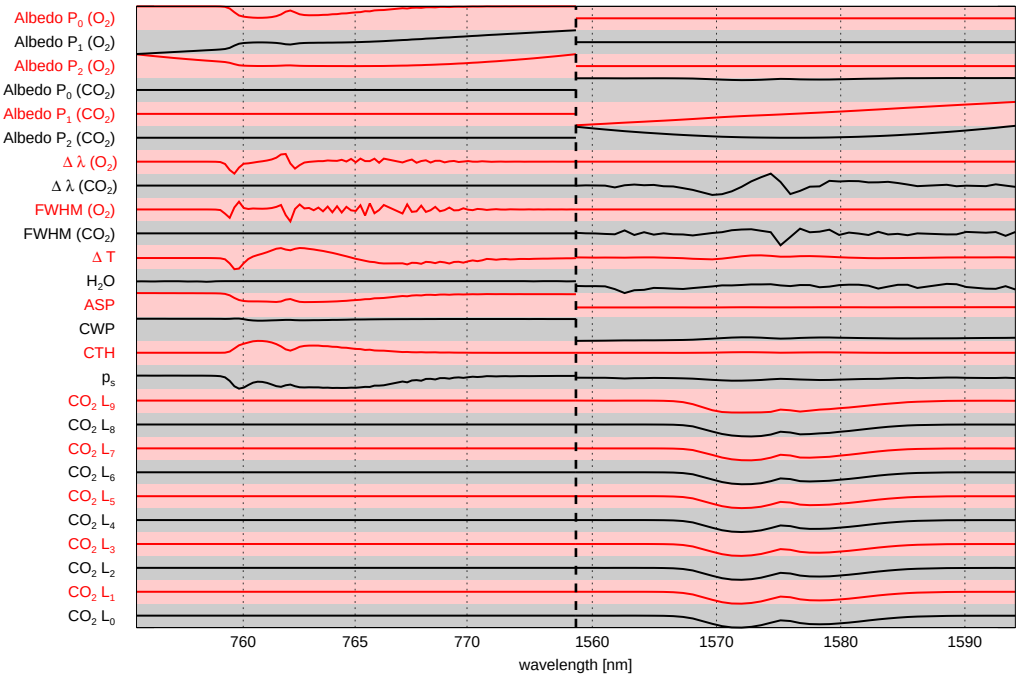

Figure 4: Weighting functions (scaled to the same amplitude) calculated with the SCIATRAN 3.2 radiative transfer code for the first guess state vector of the "met. 1σ" scenario at 40° solar zenith angle.

both fit windows. In order to get good first guess and a priori estimates for the 0^{th} polynomial coefficients, the look-up table based albedo retrieval described by Schneising et al. (2008) is used. This estimates the albedo within a micro window not influenced by gaseous absorption lines at one edge of each fit window assuming a cloud free atmosphere with moderate aerosol load.

3.2.3 CO_2 Mixing Ratio Profile

The CO_2 mixing ratio is fitted within 10 atmospheric layers, splitting the atmosphere in equally spaced pressure intervals normalized by the surface pressure p_s $(0.0, 0.1, 0.2, \ldots, 1.0)$.

CarbonTracker data over land surfaces of the years 2003 to 2005 have been analyzed in order to determine a static a priori statistic for the CO_2 mixing ratio in corresponding pressure levels. The resulting a priori state vector elements, their standard deviation and correlation matrix are shown in Fig. 5. It is not

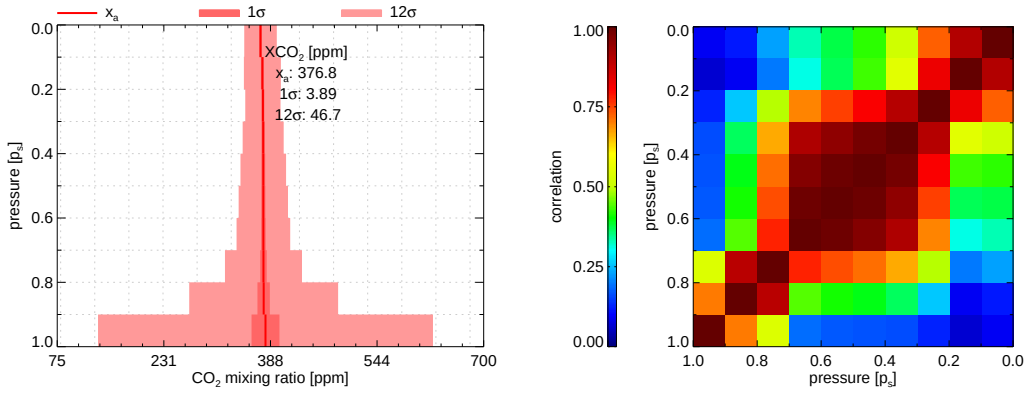

Figure 5: Static a priori knowledge of the ten-layered CO_2 mixing ratio profile calculated from three years (2003 - 2005) CarbonTracker data over land surfaces. **Left**: A priori state vector values and their 1σ and 12σ uncertainties. **Right**: Correlation matrix.

surprising that the largest variability is observed in the lowest 10% of the atmosphere. From the correlation matrix it is also visible that there are large cross correlations in the boundary layer, the free troposphere, and the stratosphere.

As the shape of the CO_2 weighting functions in SCIAMACHY resolution shows only minor changes with height, it cannot be expected that there is much information obtainable about the CO_2 profile shape from SCIAMACHY nadir measurements. Therefore, a relatively narrow constraint for the profile shape but simultaneously a rather weak constraint for XCO_2 is used. For this reason, the CO_2 part of the a priori covariance matrix is build by using the correlation matrix as is but using a 12 times increased standard deviation. As a result, the a priori uncertainty of XCO_2 increases from 3.9 ppm to 47 ppm. This enables the retrieval to put more weight on the measurement and less weight on the a priori information. In this way, the resulting degree of freedom for XCO_2 lies typically within an interval between 0.9 and 1.1. The average XCO_2 of all analyzed CarbonTracker profiles amounts to 376.8 ppm.

3.2.4 Atmospheric Profiles and Surface Pressure

When applying BESD to real SCIAMACHY measurements, atmospheric profiles of pressure, temperature, and humidity provided by ECMWF (European center for medium-range weather forecasts) are used for the forward model calculations as part of the parameter vector. Applying the hydrostatic assumption, the surface pressure determines the total number of air molecules within the

atmospheric column. Therefore, it is a critical parameter for the retrieval of XCO_2.

A dataset of more than 8000 radiosonde measurements of the year 2004 within $-70°\mathrm{E}$ to $55°\mathrm{E}$ longitude and $-35°\mathrm{N}$ to $80°\mathrm{N}$ latitude has been compared with corresponding ECMWF profiles. Resulting from these comparisons, the standard deviation of the temperature shift between measured and modeled temperature profiles amounts to 1.1 K. The corresponding value for a scaling of the H_2O profile is 32%. The biases are much smaller than the standard deviations. Therefore, unbiased a priori knowledge is used for the temperature profile shift and the scaling of the humidity profile.

The a priori uncertainty of the surface pressure is estimated to be 0.3%, which strongly constrains the surface pressure retrieval. This values seems to be realistic; King (2003) and Lammert et al. (2008) validated the sea surface pressure of ECMWF model analyses and found much smaller standard deviations of about 1 hPa and 0.5 hPa, respectively.

3.2.5 Scattering Parameters

Scattering can cause very complex modifications of the satellite observed radiance spectra and there is nearly an infinite amount of micro and macro physical parameters that are needed to comprehensively account for all scattering effects in the forward model. However, as illustrated in Fig. 1 and Fig. 2 it is unlikely possible to retrieve many of these parameters simultaneously from SCIAMACHY measurements in the O_2 fit window. The same applies to the CO_2 fit window which contains even less information about these parameters.

Therefore, BESD aims only at three macro physical scattering parameters having a dominant influence on the measured spectra. Their weighting functions contain sufficiently unique spectral signatures which makes them distinguishable from other weighting functions. These parameters are cloud top height, cloud water/ice path whereas water/ice stands for ice and/or liquid water, and the aerosol scaling factor for a default aerosol profile. All other scattering related parameters are not part of the state vector but only part of the parameter vector and are set to constant values.

The parameter vector defines that scattering at particles takes place in a plane parallel geometry at one cloud layer with a geometrical thickness of 0.5 km homogeneously consisting of fractal ice crystals with 50 µm effective radius. In addition scattering happens at a standard LOWTRAN summer aerosol profile with moderate rural aerosol load and Henyey-Greenstein phase function. Both cloud parameters are aimed at optically thin cirrus clouds because on the one

hand it is not possible to get enough information from below an optically thick cloud and on the other hand the foregoing cloud screening filters already the optically thick clouds. Additionally, Schneising et al. (2008) found that thin cirrus clouds are most likely the reason for shortcoming of the WFM-DOAS 1.0 CO_2 retrieval on the southern hemisphere.

The a priori value of CTH is set to 10 km with a one sigma uncertainty of 5 km. Both values are only rough estimates for typical thin cirrus clouds. Nevertheless, the size of the one sigma uncertainty seems to be large enough to avoid over-constraining the problem as it covers large parts of the upper troposphere where these clouds occur.

All micro physical cloud and aerosol parameters are assumed to be constant and known. This assumption is obviously not true. Scattering strongly depends on the size of the scattering particles e.g. scattering is more effective at clouds with smaller particles. For this reason, it is not possible to derive the correct cloud water/ice path without knowing the true phase function, scattering, and extinction coefficient of the scattering particles. Hence, the cloud water/ice path parameter, which is part of the state vector, is rather an effective cloud water/ice path corresponding to the particles defined in the parameter vector. As an example, it can be expected that the retrieved CWP will be larger than the true CWP in cases with true particles that are smaller than the assumed particles. Such effects must be considered when choosing the a priori constraints of CWP. Additionally, the constraints must be weak enough to enable cloud free cases with CWP $= 0$. Therefore, an a priori value for CWP of $5\,\mathrm{g/m^2}$ with an one sigma uncertainty of $10\,\mathrm{g/m^2}$ is used, corresponding to cloud optical depths τ in the range of 0 to 0.5. For the aerosol scaling factor an a priori value of 1.0 with a standard deviation of 1.0 is used.

Obviously, three parameters are by far not sufficient to describe all forms of scattering that can influence the SCIAMACHY measurements. However, BESD is not aiming to retrieve a very accurate and complete set of cloud or aerosol parameters. Therefore, as major topic of Sec. 4 the question how the lack of knowledge about several macro and micro physical cloud properties affects the XCO_2 results will be addressed.

3.3 XCO_2

This section describes how XCO_2 is calculated from the retrieved state vector elements and what implications this calculations have for the error propagation. As mentioned before, the CO_2 mixing ratio profile consists of ten layers with equally spaced pressure levels at $(0.0, 0.1, 0.2, \ldots, 1.0)p_s$. Under the assump-

tion of hydrostatic equilibrium, each layer consists of approximately the same number of air molecules. The layer weighting vector **w** is defined as fraction of air molecules in each layer compared to the whole column. In this case its value is always 0.1. For all elements that do not correspond to a CO_2 mixing ratio profile element in the state vector, the layer weighting vector is zero. XCO_2 is than simply calculated by:

$$XCO_2 = \mathbf{w}^T \hat{\mathbf{x}} \tag{13}$$

Following the rules of error propagation, the variance of the retrieved XCO_2 is given by:

$$\sigma^2_{XCO_2} = \mathbf{w}^T \hat{\mathbf{S}} \mathbf{w} \tag{14}$$

Note: the surface pressure weighting function is defined in that way, that a modification of the surface pressure influences the number of molecules in the lowest layer only. This means, after an iteration that modifies the surface pressure, the surface layer will not have the same number of air molecules anymore. The surface pressure weighting function expands or reduces the lowest layer assuming that this layer has a CO_2 mixing ratio given by the latter iteration or the first guess value. Therefore, the surface pressure weighting function influences the mixing ratio which is now a weighted average of the mixing ratio before and after iteration. For this reason, at the end of each iteration, the new non-equidistant CO_2 mixing ratio profile, which now starts at the updated surface pressure, is interpolated to ten equidistant pressure levels whereas XCO_2 is conserved.

3.4 Post-Processing

BESD has some post-processing filters which reject potentially corrupted results: i) The retrieved 0^{th} order polynomial of the albedo within the O_2 fit window must be within 0.06 and 0.6. ii) The retrieved 0^{th} order polynomial of the albedo within the CO_2 fit window must be within 0.08 and 0.8. iii) The relative RMS of the O_2 fit residual must be smaller than 1.50%. iv) The relative RMS of the CO_2 fit residual must be smaller than 0.45%.

Nevertheless, first global maps showed spurious relatively systematic bias patterns with strong correlations with the retrieved state vector elements O_2-Albedo P_0 (α_{P0}^{O2}), CO_2-Albedo P_0 (α_{P0}^{CO2}), CO_2-Albedo P_1 (α_{P1}^{CO2}), CO_2-Albedo P_2 (α_{P2}^{CO2}), and also with the surface elevation z_0 and the solar zenith angle Θ.

Under the assumption that the difference to an interpolated, smoothed field of TCCON measurements should ideally show now correlations to e.g. the solar zenith angle, a simple linear empirical correction XCO_2^c (similar to the

approach of Wunch et al. (2011)) has been developed explaining more the 70% of the deviation:

$$\begin{aligned} XCO_2^c &= 4.464\,\text{ppm} - 16.31\,\text{ppm}\,\alpha_{P0}^{O2} \\ &\quad -20.73\,\text{ppm}\,\alpha_{P0}^{CO2} - 180.2\,\text{ppm}\,\alpha_{P1}^{CO2} + 5290\,\text{ppm}\,\alpha_{P2}^{CO2} \\ &\quad +3.582\,\text{ppm/km}\,z_0 - 0.08135\,\text{ppm}/^\circ\,\vartheta \end{aligned} \tag{15}$$

This correction is applied to each retrieval passing the quality criteria.

4 Error Characterization

Within this section, BESD is applied to SCIAMACHY measurements simulated with the forward model described in Sec. 3.1 using a modified US-standard atmosphere. The corresponding measurement error covariance matrices are assumed to be diagonal. They are calculated for an exposure time of 0.25 s using the instrument simulator that was also used for the calculations of Reuter et al. (2010) and Buchwitz and Burrows (2004). The SCIAMACHY level 1b measurement errors agree well in terms of their magnitude with the simulated noise values.

However, as discussed by Reuter et al. (2011), the noise values have to be up-scaled in order to obtain optimal convergence behavior (for the application to measured SCIAMACHY data) because the observed residuals are considerably larger than expected from the SCIAMACHY level 1b measurement errors or the simulated noise levels. This is consistent with the findings of Bösch et al. (2006) who found residuals with a root mean square (RMS) difference of about 0.5% between fitted and measured SCIAMACHY radiances. These values are also similar to the filter criteria used by Schneising et al. (2008) and **?**, who reject retrievals with RMS values exceeding 0.25% in the CO_2 or 2% in the O_2 fit window. Bösch et al. (2006) discussed several physical phenomena but also instrumental effects which may contribute to this discrepancy. Up-scaling the original errors of the SCIAMACHY data achieves consistency with the expected residuals.

Anticipating, when applying BESD to measured SCIAMACHY data, Reuter et al. (2011) found that the residuals have strong systematic components. As a result, the observed stochastic errors are much smaller then estimated. Therefore, Reuter et al. (2011) scales the estimated XCO_2 errors by a factor of 0.22. In this way, the individual XCO_2 error bars still vary realistically relative to each other, e.g. with albedo but their average corresponds to 2.5 ppm, which corresponds to the single measurement precision found in the validation study. This error-scaling, however, will be applied only in Sec. 5.

In the following, the retrieval's capability to reproduce the state vector elements as well as the retrieval's sensitivity to cloud related parameter vector elements is analyzed. Therefore, a set of 35 test scenarios is defined. Some of them are only aiming at the retrieval's capability to reproduce changes of state vector elements.

However, radiative transfer through a scattering atmosphere can be very complex. Thinking about the almost infinite number of possible ensembles of scattering particles, all with different phase functions, extinction, and absorption coefficients, a set of three scattering related state vector elements is by far not enough to comprehensively describe all possible scattering effects. For this reason, the remaining test scenarios are used to estimate the sensitivity to cloud micro and macro physical parameters which are not part of the state vector but of the parameter vector.

An overview of the results of all test scenarios is given in Tab. 3 showing the systematic and stochastic XCO_2 errors of all scenarios for the solar zenith angles (SZA) 20°, 40°, and 60°. Additionally, the systematic and stochastic errors of the scattering parameters and the surface pressure are given for 40° SZA.

Note: The stochastic errors represent the a posteriori errors based on the assumed measurement noise and the assumed a priori error covariance matrix. According to Eq. (3.16) of Rodgers (2000), the systematic errors given in Table 3 correspond to the smoothing error $(\mathbf{A}-\mathbf{I})(\mathbf{x}_t-\mathbf{x}_a)$ of the state vector elements. This applies to all scenarios in which only state vector elements but no parameter vector elements are modified. In these cases, errors due to noise, unknown parameter vector elements, and due to the forward model do not exist.

4.1 The "dry run" Scenario

The true state vector of the "dry run" scenario is almost identical to the first guess state vector which is again identical to the a priori state vector in almost all elements. Only the constant part of the albedo polynomials of the first guess state vector differ slightly from the true state vector as it is estimated by the prior first guess albedo retrieval mentioned in Sec. 3.2.2. Residuals with relative root mean square (RMS) values below 0.1‰ in the O_2 and CO_2 region as well as almost no systematic errors prove that the algorithm is self-consistent (Tab. 3).

Table 3: Overview of the retrieval performance for 35 test scenarios based on SCIATRAN 3.2 simulations with a modified US-standard atmosphere. For all scenarios, we assume a Lambertian surface with an albedo which is spectrally constant 0.2 except for the "spectral albedo" scenarios. The table shows the average signal to noise (SNR) and the residuals relative root mean square (RMS) in both fit windows as well as the main retrieval errors of XCO_2, scattering parameters (CWP, CTH, APS), and surface pressure. All errors are given with systematic error (bias) ±stochastic error. The scenarios are based on the "dry run" scenario (♣), the "met. 1σ" scenario (♦), and the "no cloud" scenario (♥). Some scenarios are intended to quantify the retrievals capability of reproducing modifications of state vector elements (❍). The other scenarios are intended to additionally quantify the retrievals sensitivity to parameter vector elements (❑) (i.e. to a imperfect forward model).

Scenario	SNR		RMS [‰]		SZA 40°					SZA 20°	SZA 60°
	O_2	CO_2	O_2	CO_2	p_s [hPa]	CWP [g/m^2]	CTH [km]	APS	XCO_2 [ppm]	XCO_2 [ppm]	XCO_2 [ppm]
dry run ❍	218	146	0.09	0.00	0 ± 3	-0.1 ± 1.2	0.1 ± 1.1	-0.0 ± 0.5	-0.0 ± 11.0	0.0 ± 10.6	-0.0 ± 12.3
met. 1σ ❍	229	140	0.26	0.44	0 ± 3	0.3 ± 0.6	0.3 ± 1.0	-1.0 ± 0.5	-3.5 ± 11.8	-3.9 ± 11.2	-1.7 ± 13.8
calibration ♣,❑	232	156	0.24	0.03	0 ± 3	2.1 ± 1.3	-0.5 ± 0.9	-0.1 ± 0.5	-0.6 ± 10.4	-0.9 ± 10.0	0.0 ± 11.6
CO_2 profile											
plus 1/3σ ♣,❍	218	146	0.08	0.08	0 ± 3	-0.0 ± 1.2	0.0 ± 1.1	-0.0 ± 0.5	-1.8 ± 11.2	-1.6 ± 10.8	-2.0 ± 12.5
plus 1σ ♣,❍	218	145	0.09	0.25	0 ± 3	-0.0 ± 1.2	0.0 ± 1.1	-0.0 ± 0.5	-5.8 ± 11.7	-5.5 ± 11.3	-6.6 ± 13.0
art. profile ♣,❍	218	146	0.08	0.06	0 ± 3	-0.0 ± 1.2	0.0 ± 1.1	-0.0 ± 0.5	-1.4 ± 11.2	-1.3 ± 10.8	-1.6 ± 12.4
Spectral albedo											
sand ♣,❍	276	256	0.32	0.46	0 ± 2	-0.8 ± 1.9	0.8 ± 1.8	-0.1 ± 0.4	-2.9 ± 7.6	-2.2 ± 7.6	-3.2 ± 8.0
soil ♣,❍	176	201	0.14	0.13	0 ± 3	-0.1 ± 0.8	0.1 ± 0.8	-0.0 ± 0.5	-0.9 ± 8.6	-0.8 ± 8.4	-0.9 ± 9.4
deciduous ♣,❍	265	105	0.64	0.27	-1 ± 2	0.3 ± 2.1	-0.2 ± 1.5	-0.2 ± 0.4	-1.4 ± 14.8	-2.2 ± 14.0	-0.4 ± 16.8
conifers ♣,❍	218	90	0.62	0.21	0 ± 3	0.5 ± 1.3	-0.4 ± 1.0	-0.1 ± 0.5	-0.8 ± 17.2	-1.1 ± 16.2	-0.3 ± 19.7
rangeland ♣,❍	216	155	0.13	0.04	0 ± 3	0.1 ± 1.2	-0.1 ± 1.0	-0.0 ± 0.5	0.2 ± 10.4	0.3 ± 10.1	0.2 ± 11.6
snow ♣,❍	510	45	0.06	0.32	0 ± 2	-0.3 ± 1.7	0.2 ± 1.3	0.0 ± 0.4	0.0 ± 33.5	0.3 ± 31.9	-0.7 ± 36.5
ocean ♣,❍	88	36	0.08	0.05	0 ± 3	0.0 ± 0.6	0.0 ± 0.6	-0.0 ± 0.5	0.3 ± 38.8	0.2 ± 38.0	0.5 ± 40.3
Macro physical cloud properties											
no cloud ♣,❍	210	157	2.36	3.48	0 ± 2	0.0 ± 1.3	9.2 ± 4.9	-0.0 ± 0.4	0.3 ± 10.7	-0.2 ± 10.5	0.2 ± 11.4
cwp 0.3 ♣,❍	210	156	0.04	0.00	0 ± 2	-0.1 ± 1.3	-0.7 ± 4.9	-0.0 ± 0.4	0.1 ± 10.7	-0.2 ± 10.4	0.0 ± 11.4
cwp 3.0 ♣,❍	212	153	0.04	0.00	0 ± 2	0.1 ± 1.8	-0.1 ± 3.8	-0.0 ± 0.4	-0.0 ± 10.7	-0.0 ± 10.5	-0.0 ± 11.6
cwp 30.0 ♣,❍	245	130	1.82	0.35	-3 ± 3	-0.9 ± 0.6	0.3 ± 0.2	-0.5 ± 0.5	5.9 ± 13.1	1.3 ± 11.6	0.2 ± 16.0
cth 3 ♣,❍	216	146	0.41	0.04	0 ± 2	-9.2 ± 1.7	6.0 ± 4.8	0.0 ± 0.4	0.4 ± 11.2	0.9 ± 10.9	-1.2 ± 11.9
cth 6 ♣,❍	217	146	0.54	0.01	0 ± 3	-0.9 ± 2.8	0.4 ± 1.5	-0.1 ± 0.5	0.0 ± 10.9	0.7 ± 10.7	0.1 ± 12.0
cth 12 ♣,❍	219	146	0.06	0.01	0 ± 3	0.0 ± 0.9	-0.1 ± 1.1	0.0 ± 0.5	0.2 ± 11.0	0.1 ± 10.6	0.2 ± 12.4
cth 21 ♣,❍	221	146	0.72	0.02	0 ± 3	0.5 ± 0.7	-2.9 ± 2.1	0.1 ± 0.4	0.0 ± 11.1	-0.1 ± 10.6	0.5 ± 12.7
cfc 50 ♦,❑	220	148	0.89	0.31	-1 ± 3	-3.3 ± 0.9	-3.1 ± 0.9	-1.4 ± 0.4	-12.2 ± 11.1	-7.7 ± 10.8	-8.2 ± 12.5
cgt ♦,❑	228	140	0.26	0.45	0 ± 3	0.1 ± 0.7	-1.1 ± 0.8	-1.0 ± 0.5	-3.5 ± 11.8	-3.8 ± 11.2	-1.9 ± 13.7
multilayer ♦,❑	226	140	0.37	0.44	0 ± 3	-1.5 ± 1.0	0.6 ± 0.7	-1.0 ± 0.5	-3.4 ± 11.6	-3.3 ± 11.2	-2.5 ± 13.3
Micro physical cloud properties											
ice frac. 100 ♦,❑	220	147	0.32	0.44	0 ± 3	-5.9 ± 0.8	0.1 ± 1.8	-0.9 ± 0.4	-1.8 ± 11.3	-4.4 ± 10.9	6.0 ± 12.8
ice frac. 300 ♦,❑	213	152	0.76	0.42	1 ± 2	-11.1 ± 0.9	-1.6 ± 3.7	-0.9 ± 0.4	-3.8 ± 11.1	-5.3 ± 10.7	1.1 ± 12.1
ice hex. 25 ♦,❑	226	148	0.27	0.46	0 ± 3	5.1 ± 0.7	0.4 ± 1.2	-1.0 ± 0.5	-0.1 ± 11.3	-7.4 ± 10.5	4.9 ± 12.9
ice hex. 50 ♦,❑	220	146	0.29	0.46	0 ± 3	1.7 ± 0.8	-0.3 ± 1.6	-1.0 ± 0.4	-0.4 ± 11.4	-4.9 ± 10.7	7.5 ± 12.9
water 6 ♦,❑	225	167	0.98	0.32	-1 ± 2	2.0 ± 4.1	4.0 ± 2.8	-1.3 ± 0.4	-9.7 ± 10.2	-12.8 ± 9.8	-8.7 ± 11.4
water 12 ♦,❑	217	161	0.45	0.38	0 ± 2	-1.4 ± 1.3	7.1 ± 4.7	-1.0 ± 0.4	-6.9 ± 10.7	-5.0 ± 10.5	-0.9 ± 11.9
water 18 ♦,❑	215	159	0.41	0.39	0 ± 2	-1.6 ± 1.4	6.8 ± 4.7	-1.0 ± 0.4	-6.2 ± 10.8	-4.8 ± 10.6	-0.7 ± 11.9
Aerosol											
opac background ♥,❑	204	156	22.67	25.21	0 ± 2	0.0 ± 1.9	8.0 ± 4.4	-0.1 ± 0.4	-1.3 ± 10.5	-0.2 ± 10.4	-0.1 ± 11.4
opac urban ♥,❑	204	155	4.94	7.62	0 ± 2	0.0 ± 0.9	8.1 ± 5.0	-0.1 ± 0.4	1.3 ± 10.8	0.4 ± 10.5	0.6 ± 11.6
opac desert ♥,❑	208	158	3.07	4.52	0 ± 2	0.0 ± 0.7	9.7 ± 5.0	0.1 ± 0.4	2.3 ± 10.7	0.4 ± 10.3	2.5 ± 11.4
extreme in bl ♥,❑	213	148	0.94	0.06	-1 ± 2	0.5 ± 4.0	7.7 ± 4.2	-0.2 ± 0.4	4.0 ± 11.1	4.5 ± 11.0	5.7 ± 11.4

4.2 The "met. 1σ" Scenario

The meteorological parameters (temperature shift, H_2O scaling, APS, CWP, CTH, p_s, and CO_2 mixing ratio) of the true state vector of the "met. 1σ" scenario differ from the corresponding values of the a priori state vector by 1/3 to 1 sigma a priori uncertainty. In detail, the true, a priori, and first guess state vector as well as the retrieved state vector and corresponding values of degree of freedom, information content, and uncertainty reduction are given for this scenario in Tab. 4.

Large uncertainty reductions greater than 0.9 are found for the albedo parameters P_0 and P_1, wavelength shift, and FWHM within the O_2 spectral region. The corresponding values of the CO_2 spectral region are somewhat smaller especially for FWHM. Temperature shift and H_2O scaling are retrieved with rather low error reductions of 0.37 and 0.22.

Similarly, the APS retrieval, with an uncertainty reduction of only 0.10, seems to be dominated by the a priori even though the corresponding constraints are weak. Accordingly, the results are extremely close to the a priori value. This can be explained by the following: The aerosol profile has its maximum in the boundary layer and scattering and absorption features of aerosol vary only slowly in the relatively narrow fit windows. Therefore, it is not surprising that the shape of the APS weighting function has similarities to the surface pressure weighting function. Additionally, the sensitivity to APS is very low due to very low absolute values of the APS weighting function. For both points see Fig. 2.

As the CO_2 layered weighting functions look very similar and as the a priori knowledge shows strong inter-correlation between the layers, the retrieved profile has also strongly correlated layers. Additionally, the retrieval shows a very low error reduction especially in the stratosphere resulting in a degree of freedom for signal of 0.97 for the whole profile. This means that only one independent information can be retrieved about the profile. The shape of the profile remains strongly dominated by the a priori statistics. See also Sects. 4.4 and 4.9.

The "met. 1σ" scenario serves as basis for several other scenarios which are mainly intended to quantify the retrievals performance under more realistic conditions including also unknown parameter vector elements, i.e. an imperfect forward model.

Compared to APS, the error reduction of CWP and CTH is much higher (> 0.9). Referring to Fig. 2, the shape of the CWP weighting function strongly depends on the specific scenario which can cause ambiguities, problems of finding suitable first guess values, and problems of the convergence behavior. The

Table 4: Detailed retrieval results of the "met. 1σ" scenario for each state vector element and for the resulting XCO_2. The meaning of the columns from left to right is: 1) name of the state vector element, 2+3) weighting function with non-zero elements in the O_2 and CO_2 fit window, respectively, 4) true state $\mathbf{x}_t$, 5) first guess state $\mathbf{x}_0$, 6) a priori state $\mathbf{x}_a$ ±uncertainty, 7) retrieved state $\hat{\mathbf{x}}$ ±stochastic error, 8) information content H, 9) degree of freedom for signal d_s, 10) uncertainty reduction $\mathbf{r}_\sigma$.

Name	O_2	CO_2	$\mathbf{x}_t$	$\mathbf{x}_0$	$\mathbf{x}_a$	$\hat{\mathbf{x}}$	H [bit]	d_s	$\mathbf{r}_\sigma$
Albedo P_0	•		0.200	0.219	0.219 ± 0.050	0.203 ± 0.002	4.61	1.00	0.96
Albedo P_1	•		0.0000	0.0000	0.0000 ± 0.0100	0.0000 ± 0.0002	5.54	1.00	0.98
Albedo P_2	•		0.0000	0.0000	0.0000 ± 0.0010	0.0001 ± 0.0005	0.93	0.73	0.48
Albedo P_0		•	0.200	0.165	0.165 ± 0.050	0.199 ± 0.002	4.89	1.00	0.97
Albedo P_1		•	0.0000	0.0000	0.0000 ± 0.0100	0.0001 ± 0.0006	4.13	1.00	0.94
Albedo P_2		•	0.0000	0.0000	0.0000 ± 0.0010	0.0001 ± 0.0009	0.21	0.25	0.14
$\Delta\lambda$ [nm]	•		0.000	0.000	0.000 ± 0.100	0.000 ± 0.001	6.39	1.00	0.99
$\Delta\lambda$ [nm]		•	0.000	0.000	0.000 ± 0.100	0.005 ± 0.047	1.10	0.78	0.53
FWHM [nm]	•		0.450	0.450	0.450 ± 0.050	0.450 ± 0.003	3.99	1.00	0.94
FWHM [nm]		•	1.400	1.400	1.400 ± 0.100	1.395 ± 0.090	0.15	0.18	0.10
ΔT [K]	•	•	1.1	0.0	0.0 ± 1.1	0.3 ± 0.7	0.67	0.60	0.37
H_2O [‰]	•	•	2.93	2.22	2.22 ± 0.93	2.47 ± 0.72	0.36	0.40	0.22
APS	•	•	2.0	1.0	1.0 ± 0.5	1.0 ± 0.5	0.14	0.18	0.10
CWP [g/m^2]	•	•	15.0	10.0	5.0 ± 10.0	15.3 ± 0.6	3.95	1.00	0.94
CTH [km]	•	•	15.0	10.0	10.0 ± 5.0	15.3 ± 1.0	2.34	0.96	0.80
p_s [hPa]	•	•	1013	1013	1013 ± 3	1013 ± 3	0.04	0.05	0.03
CO_2 L_9 [ppm]		•	381.0	373.0	372.9 ± 23.9	375.2 ± 22.8	0.00	0.01	0.04
CO_2 L_8 [ppm]		•	384.6	375.6	375.7 ± 27.1	378.1 ± 26.0	0.01	0.01	0.04
CO_2 L_7 [ppm]		•	385.2	376.4	376.4 ± 25.8	380.7 ± 22.7	0.02	0.02	0.12
CO_2 L_6 [ppm]		•	386.8	376.8	376.8 ± 30.1	382.9 ± 24.7	0.02	0.03	0.18
CO_2 L_5 [ppm]		•	388.1	377.0	377.0 ± 33.4	383.9 ± 27.2	0.03	0.04	0.19
CO_2 L_4 [ppm]		•	389.1	377.0	377.0 ± 36.1	384.7 ± 29.3	0.03	0.04	0.19
CO_2 L_3 [ppm]		•	390.3	377.1	377.1 ± 39.3	385.7 ± 31.5	0.04	0.05	0.20
CO_2 L_2 [ppm]		•	396.4	377.3	377.3 ± 56.4	395.5 ± 30.2	0.08	0.10	0.46
CO_2 L_1 [ppm]		•	413.7	377.6	377.6 ± 109.1	413.7 ± 57.1	0.16	0.20	0.48
CO_2 L_0 [ppm]		•	461.7	380.2	380.2 ± 245.4	461.4 ± 133.1	0.46	0.47	0.46
XCO_2 [ppm]			397.7	376.8	376.8 ± 46.7	394.2 ± 11.8	2.12	0.97	0.75

retrieval's sensitivity to CWP and CTH is described in more detail in Sec. 4.6.

The surface pressure is retrieved with a bias of 4 hPa, a stochastic error of 6 hPa and an error reduction of 0.80. As the CO_2 layered weighting functions look very similar and as the a priori knowledge shows strong inter-correlation between the layers, the retrieved profile has also strongly correlated layers. Additionally, the retrieval shows a very low error reduction especially in the stratosphere resulting in a degree of freedom for signal of 1.07 for the whole profile. This means that only one independent information can be retrieved about the profile. The shape of the profile remains strongly dominated by the a priori statistics. See also Sec. 4.4 and Sec. 4.9.

4.3 Calibration

In contrast to other DOAS techniques, BESD uses no additional polynomial to account for spectrally smooth variations of the surface albedo and for calibration errors causing a scaling of the sun-normalized radiance. BESD uses a slightly different approach by fitting the albedo with a 2^{nd} order polynomial. The "calibration" scenario estimates the influence of calibration errors that cause an intensity scaling. For this purpose, the simulated intensity of the "dry run" was scaled by a factor by 10%. This primarily affects the retrieved 0^{th} order albedo polynomials which are approximately 10% too large. The weighting function of the 0^{th} order albedo polynomial shows similarities with other weighting functions (Fig. 4) which affects the retrieval errors of other parameters. However, the systematic errors of XCO_2 remain smaller than 1 ppm.

4.4 CO_2 Profile

The detailed results of the "met. 1σ" scenario, given in Tab. 4, already show that it is not possible to retrieve much information about the profile shape. Fig. 6 shows the retrieved CO_2 profiles of the "plus $1/3\sigma$", "plus 1σ", and "art. profile" CO_2 profile scenarios. The three scenarios differ from the "dry run" scenario only by a modified (true) CO_2 profile.

The "plus $1/3\sigma$" scenario has a true CO_2 profile which differs from the a priori profile by an enhancement of $1/3\sigma$ a priori uncertainty in each layer. A slight overestimation of the CO_2 mixing ratio is found in the boundary layer compared to an almost neutral behavior between $0.8\,p_s$ and $0.3\,p_s$, and a slight underestimation in the stratosphere. The resulting XCO_2 has a bias of -1.8 ppm and a stochastic error of 11.2 ppm for 40° SZA (Tab. 3).

In the case of the "plus 1σ" scenario, the observed effects become more pronounced. A weak overestimation is found in the boundary layer, a week

underestimation is found between $0.8\,p_s$ and $0.3\,p_s$, and a clear underestimation is found in the stratosphere. The resulting XCO_2 has a bias of -5.8 ppm and a stochastic error of 11.7 ppm (Tab. 3). Even though this scenario is a clear outlier in terms of the a priori statistics, the algorithm is still able to retrieve XCO_2 with a systematic absolute error of 1.5%. This means that the XCO_2 retrieval is still dominated by the measurement but not by the a priori constraint. However, low uncertainty reductions in the stratospheric layers as well as the fact that the retrieved mixing ratios are much closer to the a priori than to the true profile show that the stratospheric layers are dominated by the a priori information and not by the measurement.

In order to illustrate that it is actually not possible to retrieve the shape of the CO_2 profile, BESD has been confronted with an artificial profile with an almost constant mixing ratio of 380 ppm in all layers except the third layer having a mixing ratio of about 495 ppm. In this case, the retrieved CO_2 profile follows not the true profile. In fact, the retrieved profile still adopts the shape from the a priori information even though the direction of the profile modification is retrieved correctly. However, the a priori information of the CO_2 profile, which has been generated from CarbonTracker data, hint that the profile shape is already relatively well known before the measurement (Fig. 5). Therefore, it is most unlikely that scenarios like the "art. profile" scenario occur in reality.

Note that the systematic errors shown in this subsection correspond to the CO_2 profile smoothing error.

4.5 Spectral Albedo

Unfortunately, the spectral albedo cannot be assumed to be constant within the O_2 and CO_2 fit window. In the worst case, the spectral shape of the albedo would be highly correlated with the surface pressure or CO_2 weighting function. In this case, errors of the retrieved surface pressure or CO_2 mixing ratios would be unavoidable. However, this is most unlikely in reality.

As illustrated in Fig. 7, the albedo of typical surface types is spectrally smooth and only slowly varying within the fit windows. This applies especially to satellite pixels with large foot print size consisting of a mixture of surface types. Therefore, it has been assumed that the albedo can be approximated within each fit window with a 2^{nd} order polynomial. In order to make a perfect retrieval with no remaining residuals theoretically possible, a 2^{nd} order polynomial is fitted in both fit windows to the spectral albedos given in Fig. 7. These polynomials have been used as true spectral albedo for the albedo scenarios "sand", "soil", "deciduous", "conifers", "rangeland", "snow", and "ocean". All other elements of

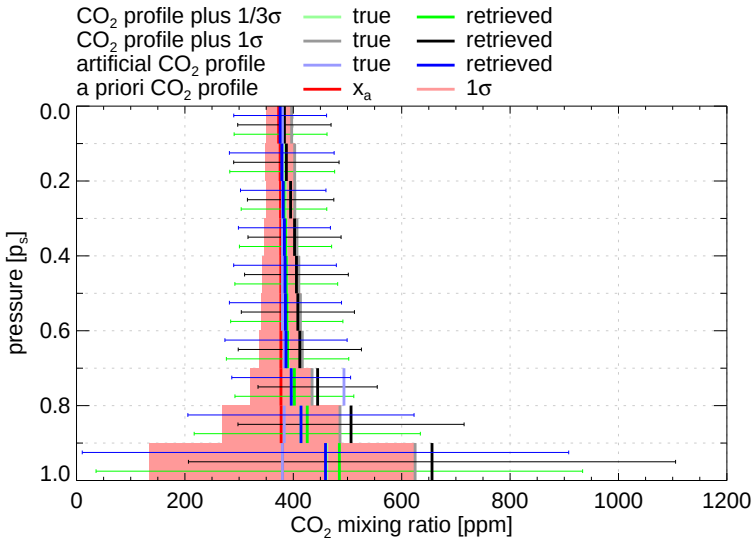

Figure 6: Retrieved and true CO_2 mixing ratio profiles of the three "CO_2 profile" scenarios.

the state vector are identical to those of the "dry run" scenario.

Tab. 3 shows that the systematic XCO_2 errors of these scenarios are in the range of -3.2 ppm and 0.5 ppm. However, most of them are close to zero. According to the large differences of the tested albedos, SNR values vary from 88 to 510 in the O_2 fit window and from 36 to 256 in the CO_2 fit window.

The lowest stochastic XCO_2 errors are found for the "sand" scenarios. These scenario have a relatively high albedo of about 0.3 in the O_2 and 0.5 in the CO_2 fit window. For this reason the corresponding SNR values are also relatively large which is essential for low stochastic errors. On the other hand, the sand scenarios have a larger systematic error (up to -3.2 ppm) which is probably attributed to an interference with the second albedo polynomial coefficient.

The largest SNR values are observed in the O_2 fit window for the "snow" scenario because of the high reflectivity of snow in this spectral region. The stochastic XCO_2 error of this scenario is quite large with about 32 ppm. This can be explained by a very low SNR value in the CO_2 fit window caused by a very low reflectivity of snow in this spectral region.

The "ocean" scenario has the lowest albedo and therefore the lowest SNR value in the O_2 and CO_2 fit window. Consequently, the largest stochastic errors of about 40 ppm for XCO_2 are observed here. Comparing these values with the

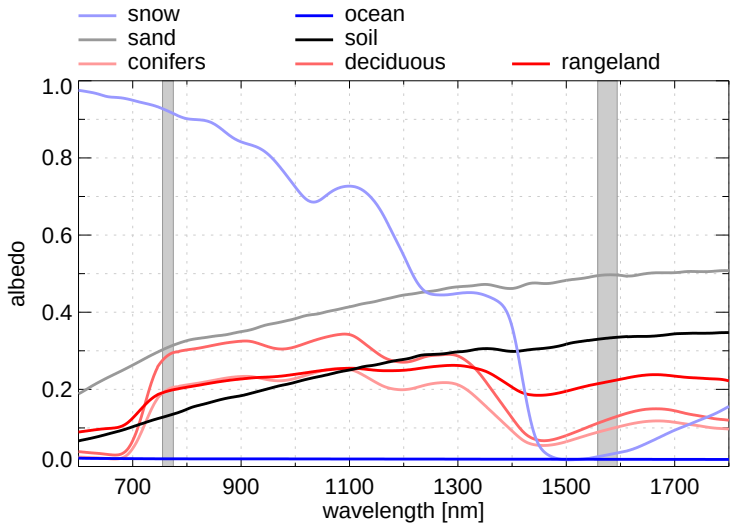

Figure 7: Spectral albedos of different natural surface types. Reproduced from the ASTER Spectral Library through the courtesy of the Jet Propulsion Laboratory, California Institute of Technology, Pasadena, California (©1999, California Institute of Technology) and the Digital Spectral Library 06 of the U.S. Geological Survey.

uncertainty of the prior knowledge shows that only very little information about XCO_2 can be obtained over snow covered or ocean surfaces.

4.6 Macro physical Cloud Parameter

Within the scenarios "no cloud", "CWP 0.3" to "CWP 30.0", the retrievals ability to retrieve CWP of an ice cloud of fractal particles with 50 µm effective radius (as defined in the parameter vector) has been tested. All other state vector elements are defined as in the "dry run" scenario. As implied by the name of these scenarios, the ice content of the analyzed clouds amounts to 0.0 g/m^2, 0.3 g/m^2, 3.0 g/m^2, and 30.0 g/m^2. The corresponding cloud optical thicknesses of these scenarios are about 0.00, 0.01, 0.10, and 1.00. Note, in this context, specifying only the optical thickness is not appropriate to describe the scattering behavior of a cloud. Knowledge about phase function, extinction, and absorption coefficients is required in order to make the optical thickness a meaningful quantity. The SNR values of the "no cloud" and "CWP 0.3" scenarios is almost identical and there are only weak differences to the "CWP 3.0" scenario. This indicates that the clouds of these cases are extremely transpar-

ent and most likely not visible for the human eye. In contrast to this, the SNR of the "CWP 30.0" scenario increases within the O_2 fit window. Within the CO_2 fit window, the effect of enhanced backscattered radiation is balanced by the strong absorption of ice in this spectral region. Nearly no systematic errors of the retrieved surface pressure can be observed except for the "CWP 30.0" scenario which results in a bias of -3 hPa in spite of its strict a priori constraint. The CWP retrieval is almost bias free compared to its stochastic error for all analyzed solar zenith angles. The same applies to the retrieved CTH of the "CWP" scenarios. For the "no cloud" scenario, the unmodified a priori value is retrieved without any error reduction which is reasonable. The stochastic CTH error reduces for CWP values greater than 3.0 g/m^2. The systematic absolute XCO_2 error of these scenarios is less or equal 0.3 ppm whereas the stochastic error is less then 12 ppm. Only the "CWP 30.0" scenarios shows larger systematic errors up to 5.9 ppm. For CWP values larger than 30.0 g/m^2 and especially for large solar zenith angles, the algorithm gets more and more convergence problems.

Analog to the "CWP" scenarios, the "CTH" scenarios are identical to the "dry run" scenario except for the cloud top height which varies between 3 km, 6 km, 12 km, and 21 km. CWP and CTH are retrieved nearly bias free for the "CTH 6", "CTH 12", and "CTH 21" scenario. The systematic XCO_2 error of these scenarios is also comparatively low with values between -0.1 ppm and 0.7 ppm. Only the "CTH 3" scenario produces larger systematic errors of CWP and CTH. Additionally, the systematic XCO_2 error of this scenario is slightly larger with values up to -1.2 ppm. This behavior may be explained by the fact that APS, and especially CTH and CWP weighing functions become more and more similar for low clouds.

Up to this point, solely the retrieval's ability to reproduce modifications to state vector elements has been tested. However, and as mentioned before, especially in respect to scattering, three state vector elements are by far not enough to entirely define the radiative transfer. For this reason, also the retrieval's sensitivity to different parameter vector elements has been analyzed with the following scenarios. At this, the focus has been put on properties of thin cirrus clouds. In the context of macro physical cloud parameters the retrieval's sensitivity to cloud fractional coverage of 50% ("CFC 50" scenario), cloud geometrical thickness ("CGT" scenario), and multilayer clouds ("multilayer" scenario) has been estimated. These three scenarios are based on the "met. 1σ" scenario. They only differ from their reference scenario by modified cloud properties.

The radiation of the "CFC 50" scenario is an average of the radiation of

the "met. 1σ" scenario with and without cloud. A systematic CWP error being $3.6\,g/m^2$ smaller than the corresponding error of the "met. 1σ" reference scenario can be observed. This can be explained with the total ice content of the "CFC 50" scenario which is $7.5\,g/m^2$ but not $15\,g/m^2$. XCO_2 values systematically differing in the range of -8.7 ppm and -3.8 ppm from those of the reference scenario are retrieved. This implies that the errors induced by fractional cloud coverage may also depend on CWP because the modeled cloud appears thicker or thinner under different solar zenith angles. The total XCO_2 errors are here in the range of -12.2 ppm and -7.7 ppm.

The "CGT" scenario differs from the reference scenario only by the cloud geometrical thickness that is 2.5 km compared to 0.5 km for the reference scenario. The results of this scenario are very similar to the reference results. Solely, the retrieved CTH is systematically 1.4 km lower. Due to the larger geometrical thickness and identical ice content at the same time, the particle density is lower. For this reason, the effective penetration depth in this cloud is larger which can explain the differences of the retrieved CTH.

The "multilayer" scenario includes two clouds with identical ice particles and identical geometrical thickness of 0.5 km. The lower CTH is 8 km whereas the upper CTH is 12 km. The corresponding "true" value, which is the basis for the calculation of the CTH bias in Tab. 3, amounts to 10 km. The results of this scenario are also comparable with the results of the reference scenario. Systematic XCO_2 differences compared to the reference scenario are in the range of 0.1 ppm and -0.8 ppm. The retrieved CTH lies between the simulated clouds and is 0.6 km larger than the average CTH of both cloud layers.

4.7 Micro physical Cloud Parameter

Within this section the retrieval's sensitivity to cloud micro physical properties is estimated. This means, BESD is confronted with clouds consisting of particles differing from those defined in the parameter vector.

The information about the three retrieved scattering parameters CWP, CTH, and APS can nearly entirely be attributed to the O_2 fit window. Scattering properties are defined within the state vector solely by these three parameters. The whole micro physical cloud and aerosol properties like phase function, extinction, and absorption coefficients are only defined in the parameter vector. Unfortunately, these micro physical properties are not known and also not constant in reality and the values that are defined in the parameter vector are obviously only a rough estimate.

Let us first consider only the O_2 fit window and assume that extinction and

absorption coefficients as well as phase function of the scattering particles are constant in this spectral region. Let us now assume two clouds having phase functions which differ only by a factor (or an offset within a logarithmic plot) outside the forward peak. In such case, the CWP retrieval would be ambiguous in respect to the micro physical properties and consequently, correct CWP values are only retrievable if the scattering particles are known. Referring to Fig. 3, the volume scattering functions within the O_2 fit window of e.g. fractal ice crystals of different size show such similarities. This means that in the case of unknown particles, it is hardly possible to retrieve the true CWP from measurements in the O_2 fit window only. The retrieved CWP is than rather an effective CWP under the assumption of specific particles. Its value does not have to correspond to the true CWP. Note: The same applies to APS and also to some extend to CTH. As long as the true geometrical thickness is known and defined in the parameter vector, the retrieved CTH corresponds to the true CTH. Nevertheless, in reality the true cloud geometrical thickness is unknown and therefore, only an effective CTH can be retrieved under the assumption of a cloud with 0.5 km geometrical thickness. This corresponds to the CTH results of the "CGT" scenario in Tab. 3.

However, the effective scattering parameters are mainly retrieved from the O_2 fit window without knowledge of the actual micro physical properties. Therefore, the retrieved parameters may not be appropriative for the usage in the CO_2 fit window under some conditions. Particularly, this depends on the relation of the absorption coefficients and volume scattering functions within the O_2 fit window compared to the CO_2 fit window. It can be expected that the retrieved parameters are applicable if this relation is similar for the true particles and those particles that are assumed within the parameter vector.

Assuming here a static relation is only a rough estimate, because methods like that of Nakajima and King (1990) are based on the fact that liquid water droplets have a stronger absorption at e.g. 1600 nm compared to e.g. 750 nm with nearly no absorption. This results in differences of the reflection at clouds in both wavelengths which can be used to derive the cloud optical thickness and simultaneously the particle's effective radius. However, this method may fail for very thin clouds under conditions with unknown spectral albedo. Additionally, ice particles usually have non-spherical shapes influencing the corresponding phase functions. For these reasons, it was not considered to retrieve the cloud particle effective radius simultaneously.

The clouds which have been used for the scenarios of this section, consist of fractal ice particles with 100 μm and 300 μm effective radius ("ice frac. 100" and "ice frac. 300" scenario), hexagonal ice particles with 25 μm and 50 μm

effective radius ("ice hex. 25" and "ice hex. 50" scenario), and water droplets with a gamma particle size distribution and an effective radius of 6 μm, 12 μm, and 18 μm, respectively ("water 6", "water 12", and "water 18" scenario). These scenarios are based on the "met. 1σ" reference scenario. The corresponding volume scattering functions are given in Fig. 3. For the most common shapes of cloud particles, a decreasing particle size results in an increasing optical thickness and a decreasing forward peak of the phase function. For this reason different true CWP values have been used for these scenarios: 3 g/m^2 for the "water" scenarios, 8 g/m^2 for the "ice hex." scenarios, and 15 g/m^2 for the "ice frac." scenarios. Additionally different CTH values have been used: 3 km for the "water" scenarios and 15 km, otherwise.

The SNR values in the O_2 fit window confirm, that more radiation is scattered back from smaller particles. However, all values are in the rage of 213 and 226. Compared to this, there is a relative large gap within the CO_2 SNR values between the ice and water scenarios. This is caused by strong absorption of ice in this spectral region which is often used for the retrieval of the cloud thermodynamic phase. This gap, however, indicates that statically defining all micro physical cloud properties in the parameter vector must result in some misinterpretations. In these cases, the enhanced or reduced back scattered radiation is mainly misinterpreted as albedo effect. Given a true albedo of 0.20 within both fit windows, the retrieved albedo varies between about 0.20 and 0.22 within both fit windows. For the retrieved surface pressure, systematic errors similar to the reference scenario are found.

The CWP behaves for ice particles as expected and shows negative biases for particles larger than 50 μm and a positive bias, otherwise. The results for water droplets are not so clear. Due to more pronounced differences in the shape of the volume scattering functions and absorption coefficients, these scenarios show increased RMS values of the resulting residuals. This especially applies to the O_2 fit window of the "water 6" scenario with a RMS value of 0.98‰. The corresponding expected RMS value due to SNR is about 4.44‰.

For CTH, moderate biases for the analyzed ice particles are found which are comparable to the bias of the reference scenario. For the water cloud scenarios, large systematic biases up to 7.1 km are found. These may be explained by a rather low true CTH of 3 km being far away from the a priori value of 10 km. Additionally, the profile of the aerosol extinction coefficient has its maximum values in the boundary layer so that misinterpretations with APS may be possible here. Large systematic and stochastic errors are found for APS, showing that the APS retrieval is mainly driven by the a priori information but also hinting that APS may easily be misinterpreted as CTH or CWP.

The systematic errors of the retrieved XCO_2 are in the range of −12.8 ppm and −4.4 ppm for 20° SZA, −9.7 ppm and −0.1 ppm for 40° SZA, and −8.7 ppm and 7.5 ppm for 60° SZA. The corresponding differences to the reference scenario are in the range of −8.9 ppm and −0.5 ppm for 20° SZA, −6.2 ppm and 3.4 ppm for 40° SZA, and −7.0 ppm and 9.2 ppm for 60° SZA.

4.8 Aerosols

Analog to the cloud scenarios, the influence of aerosol properties which are not part of the state vector have been estimated. For this purpose, BESD has been confronted with four aerosol scenarios which are described in detail by Schneising et al. (2008). Their profile, class of particles, and their phase function differ from the default aerosol scenario. The "OPAC background" scenario consists of continental relatively clean aerosol in the boundary layer and the free troposphere; the "OPAC urban" scenario has continental polluted aerosol in the boundary layer and continental average aerosol in the free troposphere; the "OPAC desert" scenario consists of desert aerosol in the boundary layer and the continental clean aerosol type in the free troposphere; the "extreme in BL" scenario has strongly enhanced urban aerosol in the boundary layer with a visibility of only 2 km and relative humidity of 99%. The "no cloud" scenario serve as basis. Except for the extreme scenario, all result are very similar to those of the "no cloud" reference scenario and the systematic absolute XCO_2 errors are below 2.5 ppm. In contrast to this, the extreme scenario produces larger systematic errors up to 5.7 ppm.

4.9 Column averaging Kernel

The averaging kernel matrix gives the sensitivity of the retrieval to the true state. Analog to this, the column averaging kernel vector $\mathbf{a}_{CO_2}$ is defined as sensitivity of the retrieved XCO_2 to the true layered CO_2 mixing ratios. In the ideal case all n_{CO_2} elements of $\mathbf{a}_{CO_2}$ would be equal 1. This would mean that a XCO_2 change introduced by a change of the i^{th} layer is one-to-one reproduced by the retrieved XCO_2. Considering only those state vector elements i corresponding to the CO_2 profile, the elements of the column averaging kernel vector can be calculated analog to Connor et al. (2008) by:

$$(\mathbf{a}_{CO_2})_i = \frac{\partial XCO_2}{\partial \mathbf{x}_i}\frac{1}{\mathbf{w}_i} = (\mathbf{w}^T\mathbf{A})_i\frac{1}{\mathbf{w}_i} \tag{16}$$

Fig. 8 shows the column averaging kernels of nine scenarios which differ by the solar zenith angles, albedo, and cloud water/ice path. All nine scenarios

are based on the "dry run" scenario. Except for the "alb. ocean" scenario, the retrieval shows a neutral sensitivity with averaging kernel values close to unity within the lower troposphere i.e. within the lowest three atmospheric layers. Within the upper atmosphere, the CO_2 absorption lines become thinner and therefore deeper due to the reduced ambient pressure so that saturation effects are more pronounced in the line centers. As a result the CO_2 weighting functions show less sensitivity in the upper atmosphere. Additionally, the a priori constraints are much tighter in this region. For these reasons, the averaging kernels of all analyzed cases reduce with height and minimum values between about 0.2 and 0.3 are found in the top layer. This behavior is similar to that found by Connor et al. (2008). Only in the third atmospheric layer between $0.3p_s$ and $0.2p_s$, a considerable increase is observed for some scenarios. Except for the CWP scenario with $0\,g/m^2$, all illustrated scenarios have an ice cloud in this layer. This increases the back scattered radiation and therefore also the sensitivity in the layers above the cloud. For bright surfaces, the relative enhancement of radiation can be neglected. In contrast to this, a major part of the detected radiation over dark surfaces is scattered at the cloud layer which increases the sensitivity above the cloud. Accordingly, the effect is more pronounced for thicker clouds, higher solar zenith angles, and lower albedos. If the fraction of backscattered radiation at the cloud layer is low enough, the effect is not observed at all.

5 Validation

5.1 Data Sets

The analyzed validation period ranges from January 2006 to December 2009. For large parts of this period, FTS measurements as well as CarbonTracker data are available at four of the TCCON (Total Carbon Column Observing Network) sites: Park Falls (USA), Bremen (Germany), Darwin (Australia), and Lauder (New Zealand). For each of these sites, three XCO_2 time series have been generated comprising SCIAMACHY, FTS, and CarbonTracker data. These time series are the basis for the validation and inter-comparison study.

5.1.1 SCIAMACHY

In the following, the data filtering procedure is described which preselects those SCIAMACHY pixels to be analyzed. All SCIAMACHY pixels falling within a radius of 350 km around each FTS station are potential candidates for the

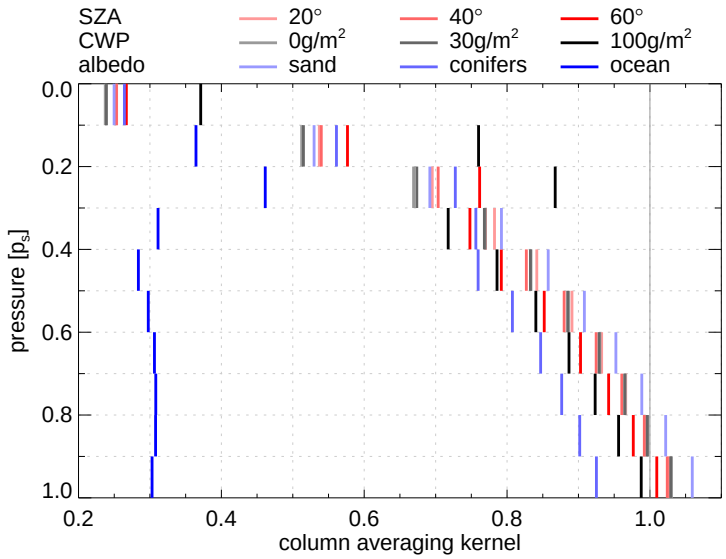

Figure 8: Column averaging kernels of nine scenarios differing by the solar zenith angles, albedo, and cloud water/ice path. All nine scenarios are based on the "dry run" scenario.

validation time series. On average these are about 70000 per FTS site. About 50000 of them have a solar zenith angle smaller than 70^o - higher solar zenith angles are excluded. Filtering for land only measurements reduces this to 14000 potential pixels. As described in section 2.2, a MERIS cloud mask is used to identify those SCIAMACHY pixels which are 100% cloud free within the SCIAMACHY pixel and within a surrounding of 40 km. After this filter, a four year time series consists of about 1400 measurements per FTS site on average.

Additionally to the regular MERIS cloud filtering, only that SCIAMACHY pixel per overpass with the largest distance to the next cloud contaminated MERIS pixel is used for validation. This prevents over-weighting of individual overpasses and meteorological situations where several pixels fulfill the cloud filter criteria. The resulting time series of SCIAMACHY measurements which are analyzed with BESD are illustrated in Fig. 9. They consists of 109 measurements at Park Falls, 63 at Bremen, 219 at Darwin, and 20 at Lauder. The data gaps around December and January result from too large solar zenith angles (Park Falls and Bremen), snow cover which is often erroneous classified as cloud (Park Falls and Bremen), and from persistent cloud coverage (Darwin). Note, because of mountains (with frequent snow cover) nearby to Lauder and because of the narrow shape of New Zealand, the 40 km criterion was relaxed

to 20 km in order to obtain data-points over Lauder.

Statistical analysis of the fit residuals shows that most residuals have a similar shape and that the stochastic fluctuations are relatively small compared to the average residual. This directly translates to retrieval errors with a relatively large systematic component and a minor stochastic component. Therefore, one can expect that the estimated errors are much larger than the actual scatter of the retrieval results. For this reason, the estimated XCO_2 errors by are multiplied by a factor of 0.22. In this way, the individual XCO_2 error bars still vary realistically relative to each other, e.g. with albedo but their average corresponds to 2.5 ppm, which is the standard deviation of all collocated differences between SCIAMACHY and FTS retrieval results. A typical fit result is shown in Fig. 10.

5.1.2 FTS

TCCON is a network of ground-based Fourier transform spectrometers recording direct solar radiation in the near-infrared with high spectral resolution (**?**). From the recorded spectra, accurate and precise column-averaged abundances of atmospheric constituents such as CO_2 are retrieved. The TCCON sites at Park Falls, Darwin, and Bremen operate a Bruker 125HR spectrometer. A similar spectrometer, a Bruker 120HR operated in Lauder over the period of this study. In order to assure comparability, all TCCON sites use the same retrieval algorithm, which is described by Washenfelder et al. (2006) and **?**. This retrieval algorithm derives XCO_2 by using a least squares fit to scale an a priori CO_2 profile. The a priori profile is derived by an empirical model based on fits to NOAA's GLOBALVIEW CO_2 data for the troposphere and follows the decrease in the stratosphere based on the age of air (Andrews et al., 2001).

Accuracy and precision of the FTS measurements have been determined in many calibration and validation campaigns with airborne in situ instruments. The single measurement precision and accuracy of the FTS instruments is better than 0.25% (**?**). The standard deviation of all cloud free measurements within one hour amounts typically to 0.1% (Washenfelder et al., 2006; Messerschmidt et al., 2010; Deutscher et al., 2010). However, the precision of the FTS measurements depends on many factors, like the solar zenith angle and scatterers in the atmosphere. Precision estimates for the individual FTS measurements are given in the FTS data files. The median precision, of the entire analyzed FTS dataset amounts to 0.6 ppm.

Wunch et al. (2010) calibrated XCO_2 of several TCCON sites against WMO-scale instrumentation aboard aircraft and found that all stations can be de-

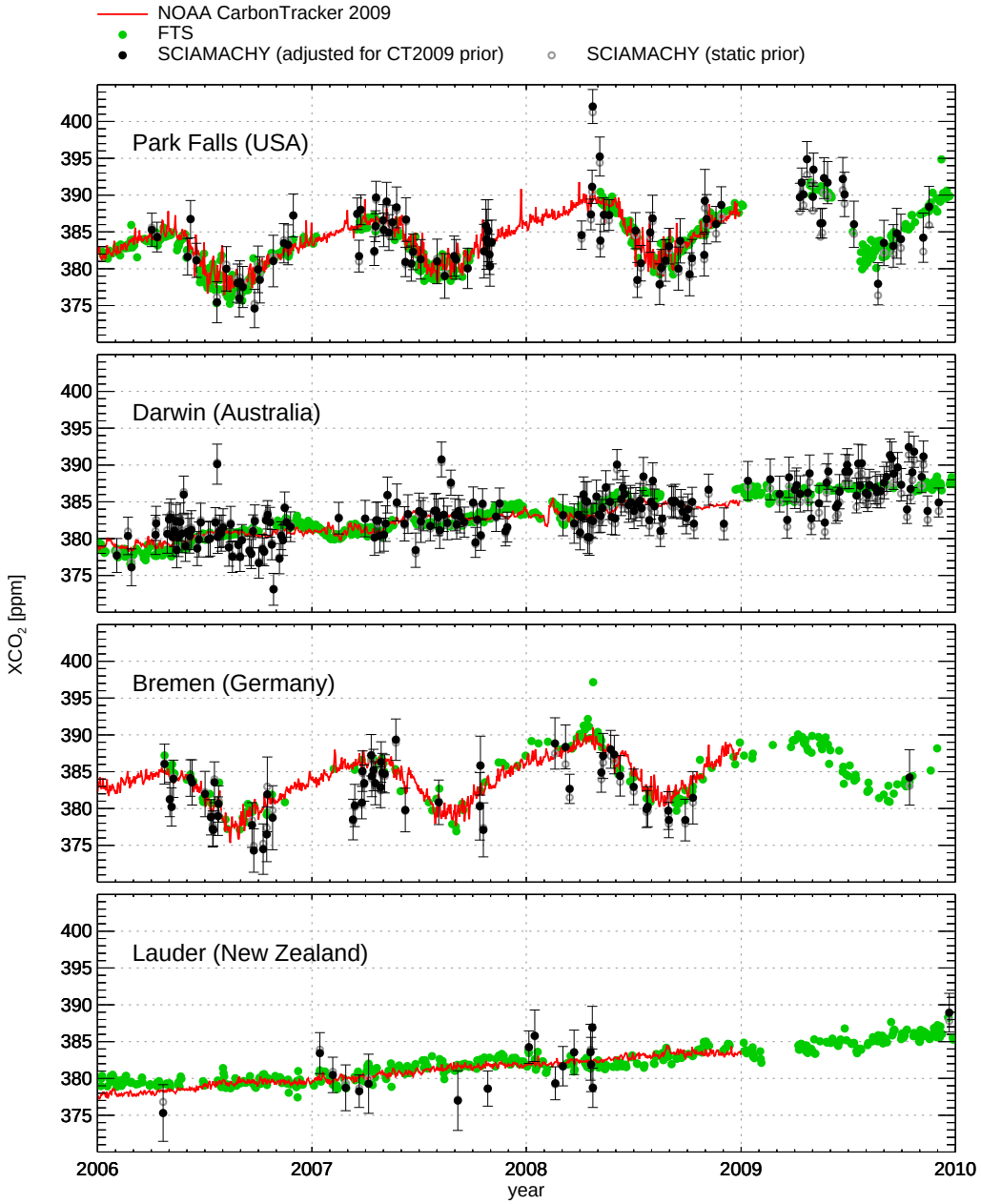

Figure 9: XCO_2 time series of individual measurements at the TCCON sites Park Falls, Darwin, Bremen, and Lauder. The corresponding statistical quantities which measure the agreement between the time series are given in Tab. 5.

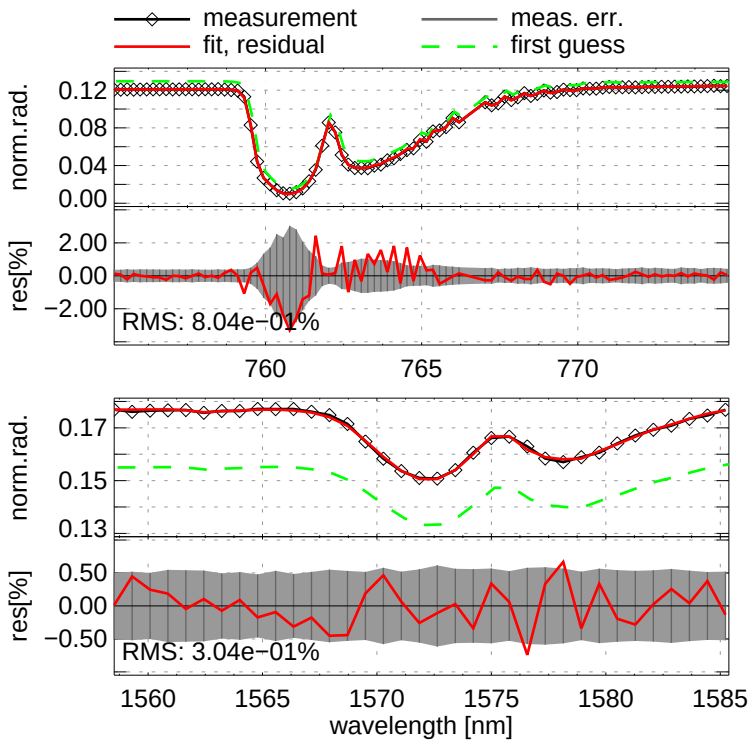

Figure 10: O_2 and CO_2 fit windows with SCIAMACHY measurements, first guess, fitted sun-normalized radiation, residual and measurement error for an exemplary SCIAMACHY pixel over Park Falls taken at April 20, 2007.

scribed by a single regression line and hence single calibration factor, with variations around the regression line. This means they found no significant systematic offsets in calibration factors between the analyzed TCCON sites. Messerschmidt et al. (2010) compared collocated identical TCCON FTS instruments and found that systematic offsets are indeed small (0.07%) as long as laser mis-samplings are eliminated.

SCIAMACHY flies on a sun synchronous orbit with an equator crossing local time of 10:00am. Due to the diurnal cycle of the atmospheric CO_2 concentration, only FTS measurements with a maximum time difference of less than two hours have been accepted. In order to further minimize the noise, all FTS measurements fulfilling this criterion have been averaged. The expected precision of the averaged FTS measurements can be neglected compared with the single measurement precision which is expected from the SCIAMACHY retrievals. Additionally, only those measurements are used which are flagged as "good".

In total, after filtering, the FTS time series consist of 540 measurements at Park Falls, 794 at Darwin, 180 at Bremen, and 459 at Lauder.

5.1.3 CarbonTracker

NOAA's CarbonTracker assimilation system predicts global 3D fields of the atmospheric CO_2 mole fraction. For this purpose, it assimilates measurements of air sampling networks and tall towers. The transport of CO_2 is simulated with the TM5 model driven by ECMWF meteorological fields. A detailed description of CarbonTracker can be found in the publication of Peters et al. (2007). For this validation study, CO_2 fields of CarbonTracker version (CT2009) have been used. CT2009 provides global data with $3^o \times 2^o$ spatial and 3 h temporal resolution spanning the time period from January 2000 to December 2008.

From the CT2009 fields, two time series from January 2006 till December 2008 have been generated. One consists of spatio-temporal collocations with the SCIAMACHY retrievals. The other consists of daily CarbonTracker values being collocated with the FTS station and temporally closest to SCIAMACHY's nadir overpassing local time. The first time series is used for all comparisons of SCIAMACHY with CarbonTracker while the second is used for comparisons between the FTS and CarbonTracker. Due to CarbonTracker's relatively coarse temporal and spatial resolution, both methods often refer to the same CarbonTracker grid box. As the resulting differences between both methods are marginal, only the second dataset with daily values at the FTS stations is shown in the figures.

5.2 Strategy

TCCON provides an essential validation resource for the Orbiting Carbon Observatory (OCO), SCIAMACHY, and GOSAT. Due to their precision and accuracy, TCCON FTS measurements can be used as ground truth for this validation study. However, CarbonTracker has been shown in evaluation studies to be close to reality (Peters et al., 2007). Therefore, comparisons between FTS and CT2009 as well as SCIAMACHY and CT2009 have additionally been performed.

The comparison of two column measurements and one model is not trivial as a result of the different averaging kernels. According to (Rodgers, 2000), a suitable way of tackling this issue is to adjust the measurements for a common a priori profile. This ensures that the differences between the analyzed data sets are not attributed to the a priori information. Here, CT2009 is used which

facilitates the comparison between all three data sets SCIAMACHY, FTS, and CT2009.

$$\mathbf{x}_{adj} = \hat{\mathbf{x}} + (\mathbf{I} - \mathbf{A})(\mathbf{x}_{CT2009} - \mathbf{x}_a) \tag{17}$$

In this equation, $\hat{\mathbf{x}}$ represents the retrieved profile of CO_2 concentrations (FTS or SCIAMACHY), $\mathbf{x}_a$ the corresponding a priori profile, $\mathbf{x}_{CT2009}$ the new (common) a priori profile, and $\mathbf{A}$ the column averaging kernel matrix. $\mathbf{A}$ is diagonal and is defined by the profile of the retrieval's sensitivity to CO_2, i.e., the column averaging kernel (vector).

When this analysis was performed, FTS averaging kernels as well as the a priori profiles of the FTS retrieval were available for the Park Falls site. However, the FTS CO_2 averaging kernels are often close to unity. Additionally, the (FTS) a priori XCO_2 does not differ much from corresponding CarbonTracker values. For these reasons, adjusting the FTS measurements as described above results only in small modifications of about 0.1 ppm in agreement with the findings of Washenfelder et al. (2006). This is small compared to SCIAMACHY's precision and as a result the adjustment of the FTS values is omitted for the three other TCCON sites.

As shown in section 4.9, the averaging kernels of BESD are in most scenarios close to unity, especially in the lower atmosphere. Values significantly lower than 0.9 are generally only found above (at pressures lower than) 500 hPa. This means that the results are dominated by the measurements and less by the a priori knowledge. However, it also means that there is some remaining influence from the a priori information. For this reason, a static a priori CO_2 profile is used which does not depend on time or location. This ensures that any variation of the retrieval results can be attributed to variations of the measurements and not to variations in the a priori information. These (non-adjusted) results will tend to slightly underestimate the magnitude of the XCO_2 variations (e.g. seasonal cycle and year-to-year increase). The differences between the original results with static a priori and those adjusted to CT2009 as common a priori profiles can be seen in Fig. 9.

Within the next section, the adjusted values have been used to derive statistical quantities such as the regional relative accuracy, single measurement precision, correlation coefficient, the year-to-year increase and the amplitude of the seasonal cycle. Many of these quantities are more valuable if they are provided together with an appropriate error estimate. For this purpose, a bootstrapping method (Efron, 1979) with a set of 100 bootstrap samples has been used to calculate the standard error of the estimated statistical quantities. Significance is assumed for differences larger than twice the standard error.

Table 5: Regional biases Δ, precision on single measurement basis σ, and correlation ρ of all collocated measurements shown in Fig. 9. The column "global" corresponds to a merged data set enclosing the data of all four sites. As described at the beginning of Sec. 5.3, a global offset correction is applied. Therefore, all biases are zero by definition in this case.

Location	SCIAMACHY vs. FTS			SCIAMACHY vs. CT2009			CT2009 vs. FTS		
	Δ [ppm]	σ [ppm]	ρ	Δ [ppm]	σ [ppm]	ρ	Δ [ppm]	σ [ppm]	ρ
Park Falls (USA)	-0.2 ± 0.4	2.5	0.83	-0.2 ± 0.3	3.0	0.77	0.1 ± 0.1	0.8	0.97
Darwin (Australia)	0.3 ± 0.2	2.4	0.69	0.4 ± 0.2	2.3	0.74	0.0 ± 0.1	0.9	0.93
Bremen (Germany)	-1.2 ± 0.6	2.6	0.61	-1.1 ± 0.6	2.5	0.73	0.1 ± 0.2	1.3	0.95
Lauder (New Zealand)	0.5 ± 0.8	2.5	0.47	0.5 ± 0.8	2.9	0.64	0.0 ± 0.4	0.9	0.86
global	0.0 ± 0.2	2.5	0.72	0.0 ± 0.2	2.7	0.74	0.0 ± 0.1	0.9	0.94

Table 6: Year-to-year increase as well as average peak-to-peak amplitude of the seasonal cycle calculated from the smoothed SCIAMACHY, FTS, and CT2009 time series shown in Fig. 11.

Location	Year-to-year increase [ppm/year]			Peak-to-peak amplitude [ppm]		
	SCIAMACHY	FTS	CT2009	SCIAMACHY	FTS	CT2009
Park Falls (USA)	1.88 ± 0.44	2.01 ± 0.05	1.96 ± 0.03	7.92 ± 0.95	7.41 ± 0.13	6.94 ± 0.08
Darwin (Australia)	2.27 ± 0.20	2.30 ± 0.03	1.99 ± 0.01	2.48 ± 0.42	1.91 ± 0.05	1.18 ± 0.02

5.3 Results

Globally uniform biases produce no artificial unrealistic XCO_2 gradients. Therefore, they are unproblematic and can simply be subtracted from the retrieved XCO_2 before further analysis. Here, for convenience, CT2009 is chosen as the baseline for the global offsets of SCIAMACHY and FTS XCO_2. Then, the average difference of all SCIAMACHY/CT2009 and FTS/CT2009 collocations is calculated. As a result, a global offset of 6.25 ppm has been added to the SCIAMACHY data set and 1.35 ppm to the FTS data set. The entire bias corrected XCO_2 time series of SCIAMACHY, FTS, and CT2009 at all four stations are shown in Fig. 9.

All results, which are related to the agreement of individual collocated measurements of two data sets i.e. their regional bias Δ, precision σ, and correlation ρ, are summarized in Tab. 5. Tab. 6 summarizes all results which are related to the seasonal cycle and the year-to-year increase.

5.3.1 Regional Biases

As mentioned earlier, undetected biases on regional scales negatively impact surface flux inverse modeling (Miller et al., 2007; Chevallier et al., 2007). Systematic differences between the four FTS sites may imply such regional scale biases. For this reason, the systematic offsets between all three data sets have been calculated separately for each station. Compared to the FTS, SCIAMACHY shows systematic differences between -1.2 ± 0.6 ppm and 0.5 ± 0.8 ppm. At all stations, the bias is smaller than (or equal) twice its standard error and smaller than its standard error at two stations. The comparison between CT2009 and FTS shows insignificant systematic differences in the range of 0.0 ± 0.4 ppm and 0.1 ± 0.2 ppm. These biases are always less than or equal their error.

5.3.2 Single Measurement Precision

Another important characteristic of the data set is the single measurement precision, which is here define as the standard deviation of the difference between two collocated data sets. With respect to the FTS, the SCIAMACHY XCO_2 single measurement precision varies between 2.4 ppm and 2.6 ppm between the four stations. Using all collocations of all stations, the global single measurement precision amounts to 2.5 ppm. This is slightly better than the 2.7 ppm obtained when comparing SCIAMACHY with CT2009. Even though the difference is not statistically significant, it indicates that SCIAMACHY may agree better with the FTS than with CT2009 even though the FTS measurements have measurement noise. Note, the three compared data sets have different spatial resolutions. Additionally, the distance between a SCIAMACHY pixel and a collocated FTS measurement can amount up to 350 km. As a result, the calculated single measurement precisions are upper bounds because they include a representation error that can exceed 0.5 ppm (Tolk et al., 2008).

5.3.3 Correlation

The correlation is a measure of the linear dependence between two data sets. Comparing SCIAMACHY with FTS, the correlation coefficient amounts globally to 0.72 and varies from station to station between 0.47 and 0.83. The correlation coefficient does depend on the range of XCO_2 sampled (seasonal cycle, year-to-year increase, and number of samples). It is therefore not surprising that the highest correlation is found at Park Falls (large seasonal cycle, large number of coincident SCIAMACHY retrievals) and the lowest at Lauder (small

seasonal cycle, only a few coincident SCIAMACHY retrievals), even though the single measurement precisions are similar.

5.3.4 Year-to-Year Increase

In order to derive the average year-to-year increase of XCO_2, a linear trend model has been fitted to the deseasonalized time series of SCIAMACHY, FTS, and CT2009. This analysis is based on the full time series instead of collocations only. More precisely, each of the four years is divided into 25 intervals. The intervals are assumed to be short enough to contain no significant seasonal component. If more than one (of the four) i^{th} interval contains data, the linear trend for the time series of the i^{th} intervals has been calculated. This means up to 25 linear trends of sub-sampled time series with no seasonal component are calculated. The year-to-year increase is then calculated from the average trend.

As a result of the low amount of SCIAMACHY data in the Bremen and Lauder time series, this analysis is restricted to Park Falls and Darwin. At Park Falls, no significant difference has been found between the year-to-year increase of SCIAMACHY (1.88 ± 0.44 ppm/a), FTS (2.01 ± 0.05 ppm/a), and CT2009 (1.96 ± 0.03 ppm/a). At Darwin, the FTS has a larger year-to-year increase of 2.30 ± 0.03 ppm/a, which agrees with the SCIAMACHY retrieved value of 2.27 ± 0.20 ppm/a. Compared to this, the year-to-year increase of CT2009, which amounts to 1.99 ± 0.01 ppm/a, is significantly smaller. However, the difference between CT2009 and FTS has a similar magnitude to SCIAMACHY's noise.

5.3.5 Seasonal Cycle

In order to analyze the seasonal cycle, smoothed representations of the XCO_2 time series (Fig. 11) have been calculated. This is achieved by convolving the original time series with a Hann function $h(x) = sin^2(2\pi x/w)$ with a total width w of four months which corresponds to an effective width of two months. The laws of error propagation are consistently applied to derive the standard error of the smoothed SCIAMACHY time series. For the same reasons as mentioned in the previous subsection, this analysis is restricted to the Park Falls and Darwin time series.

As shown in Fig. 11, the smoothed SCIAMACHY data agree most times within one standard error and nearly all the time within two standard errors with CT2009 and the FTS. In periods with frequent measurements, the standard error is considerably reduced due to the smoothing.

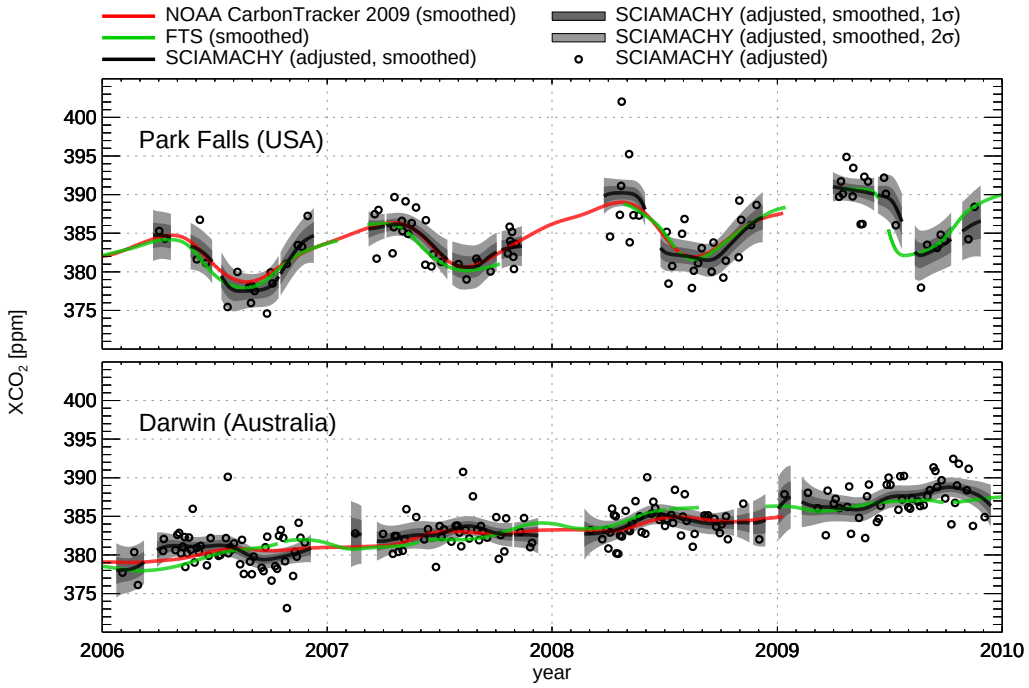

Figure 11: Smoothed representations of the time series measured at Park Falls and Darwin. The smoothing is performed by convolving the time series of Fig. 9 with a Hann function with an effective width of two months (four months in total). The gray shaded areas represent the standard error (1σ and 2σ).

After subtracting the linear trend i.e. the year-to-year increase, the average peak-to-peak amplitude of the seasonal cycles have been derived. At Park Falls the shape of the seasonal cycle in all data sets agrees well. The average peak-to-peak amplitudes amount to 7.92 ± 0.95 ppm for SCIAMACHY, 7.41 ± 0.13 ppm for the FTS, and 6.94 ± 0.08 ppm for CT2009. Due to SCIAMACHY's relatively large standard error, no significant difference between SCIAMACHY and both other data sets can be observed. However, CarbonTracker's underestimation of 0.47 ppm (compared to the FTS) lies above the level of significance.

At Darwin the seasonal cycle is less pronounced and differences are more apparent. The agreement between the shape and amplitude of the three time series varies from year to year. Relatively good agreement of all three data sets is found in the years 2007 and 2008, whereas differences are pronounced in 2006. Bearing this in mind, the peak-to-peak amplitudes can be characterized. These are 2.48 ± 0.42 ppm for SCIAMACHY, 1.91 ± 0.05 ppm for the FTS,

and 1.18 ± 0.02 ppm for CT2009. In this case, the differences of CT2009 to the FTS but also to SCIAMACHY are significant. No significant difference is found between SCIAMACHY and the FTS. Even though, the difference between SCIAMACHY and the FTS (0.57 ppm) is smaller than between CT2009 and the FTS (0.73 ppm), one should keep in mind that its magnitude is still quite large and the standard errors are much higher here.

5.3.6 Other State Vector Elements and RMS

In order to ensure that the results of other important state vector elements are also reasonable, Fig. 12 and 13 show time series of these parameters.

Albedo

The retrieved albedo has a reasonable seasonal cycle and is typically within the range of 0.1 and 0.3. The O_2-A band is located directly behind the red-edge, i.e., green vegetation has a large albedo in this spectral region. For this reason, the growing season is readily observed in the albedo within the O_2-A band at Park Falls.

Surface Pressure

As described above, the surface pressure is strongly constrained by the a priori knowledge i.e. ECMWF re-analysis. As a result of the relatively strict constraint, it is not surprising that the retrieved values follow the corresponding ECMWF values very well. However, a systematic offset of about 9.5 hPa has been observed, which is similar to the findings of Bösch et al. (2006), who attributed systematic offsets in the retrieved surface pressure to potential inadequacies of the spectroscopy.

Temperature and Humidity

ECMWF re-analyses are the first guess and the a priori knowledge for temperature and humidity. Even though these constraints are weak, good agreement between the retrieved and the modeled values has been found. The seasonal cycle agrees with the expected behavior with largest values being in summer time. The observed systematic temperature offset amounts to about -3.6 K.

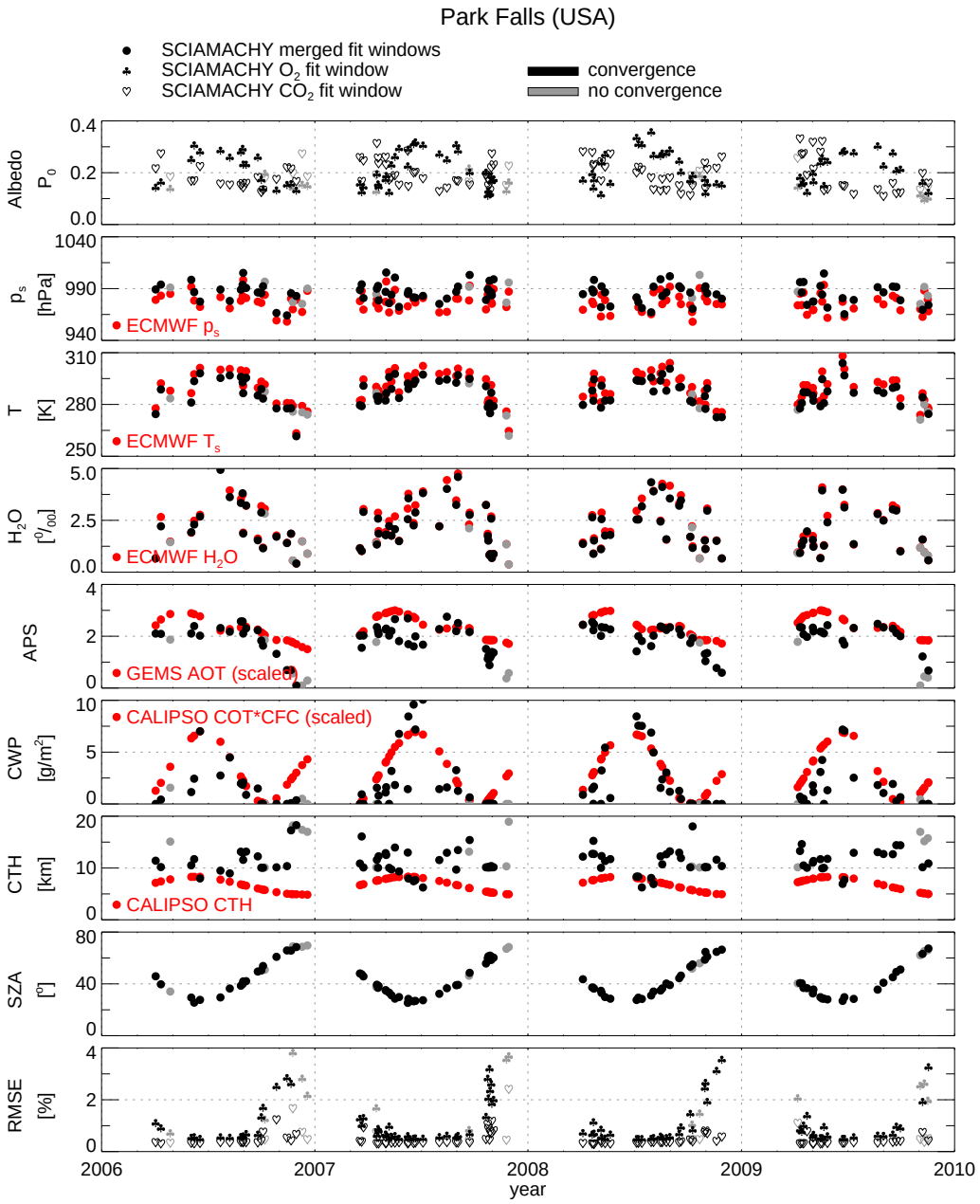

Figure 12: Park Falls time series of selected important state vector elements which are by-products of the SCIAMACHY XCO_2 retrieval. From top to bottom: albedo in both fit windows represented by the 0^{th} order polynomial, surface pressure, 2 m temperature, column-average mole fraction of water vapor, scaling factor for a default aerosol profile (APS), cloud water/ice content (CWP), cloud top height (CTP), solar zenith angle (SZA), root mean square error of the fit residual in both fit windows. Corresponding values of ECMWF, CALIPSO (2007), and GEMS (2005) are also shown.

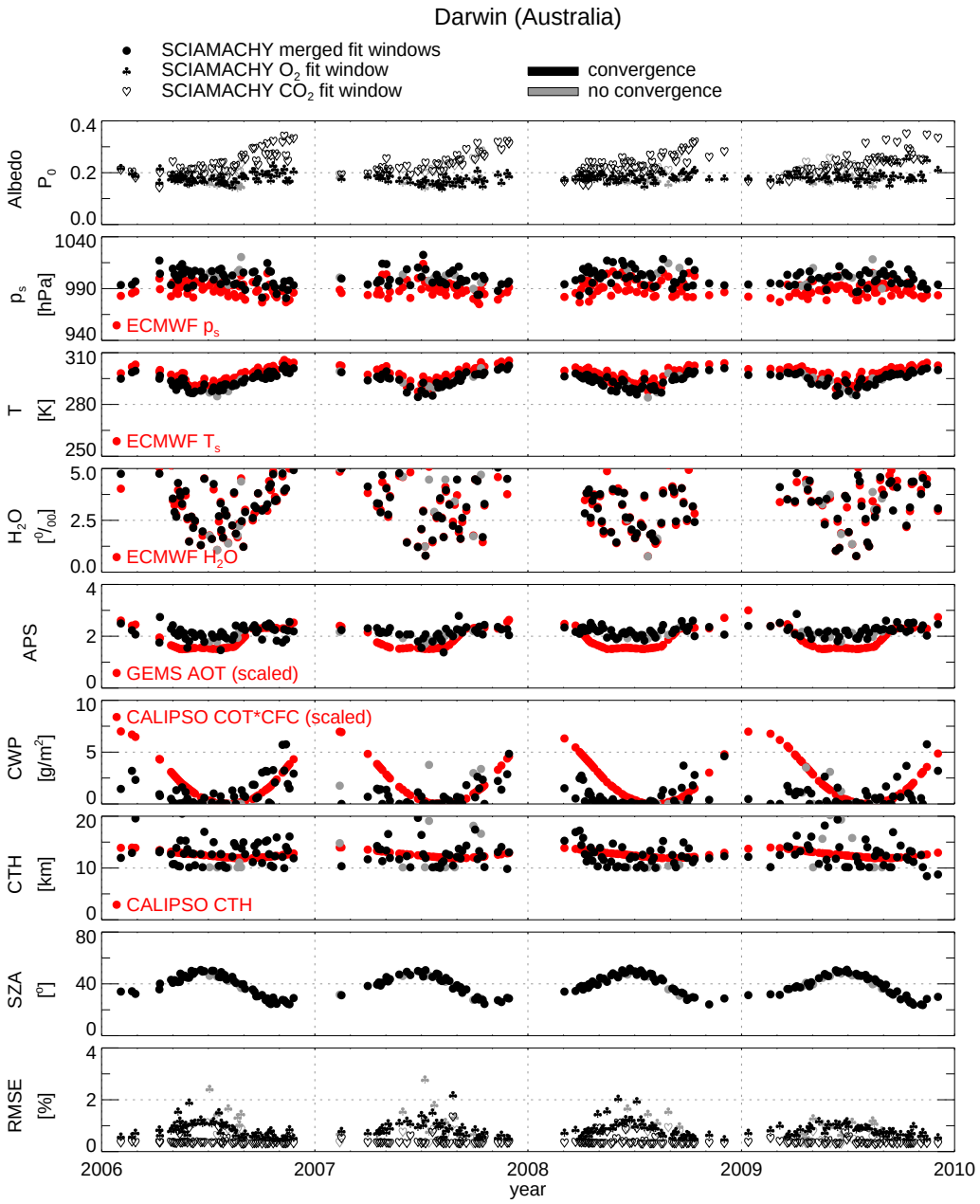

Figure 13: Darwin time series of selected important state vector elements which are by-products of the SCIAMACHY XCO_2 retrieval. From top to bottom: albedo in both fit windows represented by the 0^{th} order polynomial, surface pressure, 2 m temperature, column-average mole fraction of water vapor, scaling factor for a default aerosol profile (APS), cloud water/ice content (CWP), cloud top height (CTP), solar zenith angle (SZA), root mean square error of the fit residual in both fit windows. Corresponding values of ECMWF, CALIPSO (2007), and GEMS (2005) are also shown.

Scattering

BESD describes scattering by aerosol profile scaling (APS), the cloud ice/water path (CWP), and the cloud top height (CTH). All other scattering related parameters such as the cloud and aerosol micro physics or the aerosol profile shape are kept at default values described in section 3.

APS and CWP show a pronounced seasonal cycle with maximum values in the summer months. Qualitatively, the seasonal cycle of APS is similar to that of the GEMS AOT. GEMS stands for "Global and regional Earth-system Monitoring using Satellite and in-situ data" and the GEMS AOT product is based on the assimilation of MODIS AOT retrievals at the ECMWF.

The seasonal cycle of CWP and CALIPSO (Cloud-Aerosol Lidar and Infrared Pathfinder Satellite Observation) effective COT are also in good qualitative agreement. The effective COT being defined as cloud fractional coverage (CFC) of thin clouds, which can probably not be detected with MERIS, multiplied by COT of these clouds. The retrieved CTH shows no clear recurring seasonal cycle. However, similarities with the corresponding CALIPSO data, which shows higher values in the Tropics (Darwin) than in Park Falls, are observed.

With respect to the GEMS and CALIPSO data, used in the study, the following is to be noted: i) CWP, CTH and APS are "effective" values and a quantitative one-to-one agreement with corresponding GEMS or CALIPSO values cannot be expected (Reuter et al., 2010). Therefore, GEMS AOT and CALIPSO CWP are scaled to nicely fit into the corresponding y-axes of Fig. 12 and 13. ii) The plotted GEMS data repeatedly show the year 2005 while the CALIPSO data shown are based on repetitions of the year 2007 only. iii) Operational NASA level 2 CALIPSO data of version 2.01 has been used. The data is filter for COT values below 0.1 and measurements at night time, only. Additionally, the data is smoothed by convolution with a Gaussian kernel with a full width half maximum (FWHM) of $8^o \times 8^o \times 3$ month. This dampens out short term and small scale variations so that only the seasonal changes remain.

Fig. 14 (right) shows a SCIAMACHY pixel near Darwin taken at July 06, 2007 underlaid with a MERIS true color composite. It is an example for a typical clear sky situation. Correspondingly, a CWP of 0.0 g/m^2 and a relatively low APS value of 1.9 are retrieved. Fig. 14 (left) shows the meteorological situation around Darwin on October 09, 2006 and is an example for a situation with undetected thin cirrus clouds, which are visible in the MERIS true color composite. In this case, the retrieved values of CWP and APS are elevated and amount to 3.2 g/cm^2 and 2.4, respectively.

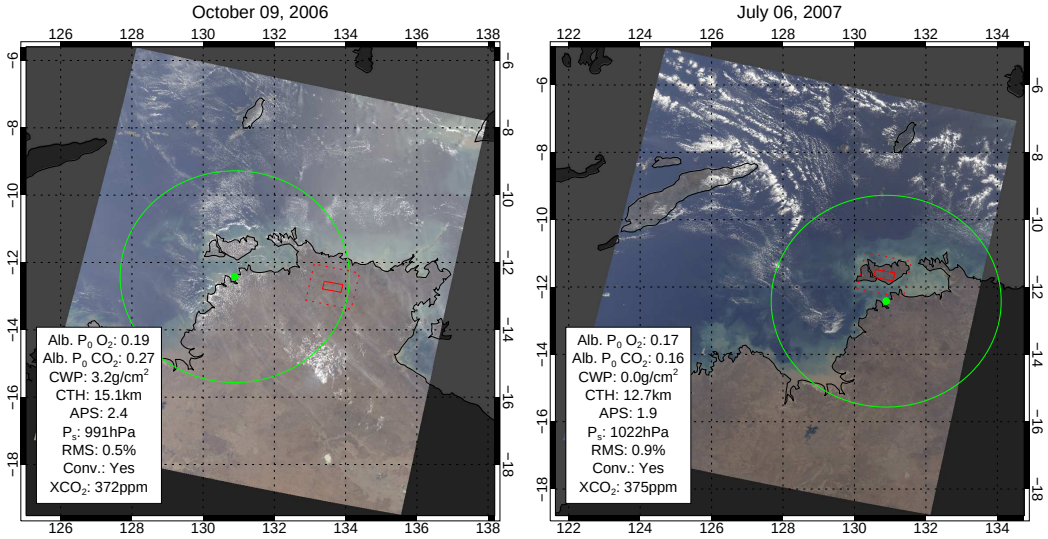

Figure 14: Meteorological situation of two exemplary SCIAMACHY measurements (red) falling in a 350 km surrounding of Darwin (green) as seen from MERIS. The SCIAMACHY pixels are encased by a 40 km cloud screening safety margin (red, dotted). A typical cloud free situation is shown on the right hand side. In contrast to this, the image on left hand side shows a situation with (undetected) cirrus clouds.

RMS

The median of the relative root mean square difference between fit and measurement amounts to 0.7% in both fit windows together. With a median of 0.3% compared to 0.8%, the fit residuals are generally smaller in the CO_2 than in the O_2 fit window. Especially the latter shows a pronounced RMS seasonality. This has two reasons: because the fit quality depends on the solar zenith angle (e.g. due to the plane parallel assumption) and because vegetated surfaces have a low albedo in the O_2 fit window out of the growing season. The latter applies presumably not for Darwin because the seasonality of vegetation is expected to be low here.

6 Limitations and Potential Improvements

Currently an issue with SCIAMACHY data version 7.0x consolidation U data is under investigation. This issue seems to result in low biased outliers in several months. First promising tests with four months of global SCIAMCHY data indicate that this problem is solved with version 7.0x consolidation W data. As

post-processing filtering is most probably not possible, a reprocessing of the full SCIAMACHY time series is planned for the future.

As discussed in Sec. 4 and also in the publication of Reuter et al. (2010), all micro-physical cloud and aerosol properties are assumed to be known. However, this is not the case and can cause XCO_2 errors as seen in Tab. 3. Including micro-physical properties such as Ångström exponent or effective droplet radius into the state vector would require an additional fit window with strong absorption features. Algorithms developed for OCO and GOSAT follow this approach. However, at preset it is not planned to adapt this for SCIAMACHY due to issues with channel 7 which would covers appropriate strong CO_2 bands.

In its current state, BESD requires computational expensive online radiative transfer calculations. Even with the strict data pre-filtering described in Sec. 2.2, the processing speed is only about four times larger than real time (using 24 state of the art CPU cores in parallel). This means that there is a clear need for improving the processing speed in order to enable timely reprocessing of the whole SCIAMACHY time series. Taking advantage of additional numerical approximations or simply increasing the number of CPUs has an estimated potential to enhance the processing speed by a factor of 5 to 20. Tabulating the radiative transfer would increase the processing speed by orders of magnitude. However, this is not trivial due to the relatively large number of state vector elements resulting in a LUT with many dimensions.

7 Summary and Conclusions

Introduction

The Bremen Optimal Estimation DOAS (BESD) algorithm is designed to analyze SCIAMACHY sun normalized radiance measurements to retrieve the column-average dry-air mole fraction of atmospheric CO_2. BESD is a so called full physics algorithm which uses measurements in the O_2-A absorption band to retrieve scattering information of clouds and aerosols. This information is transferred to the CO_2 absorption band at 1580 nm by simultaneously fitting the spectra measured in both spectral regions. The explicit consideration of scattering by this approach reduces potential systematic biases due to clouds or aerosols. The ATBD describing BESD in detail is in large parts compiled from text and figures of the publications of Reuter et al. (2010) and Reuter et al. (2011).

Measurement Vector

SCIAMACHY nadir and corresponding sun spectra of 7.xx are utilized to calculate the sun normalized radiance within the O_2 and the CO_2 fit window. The SCIAMACHY data are calibrated with ESA's SciaL1C calibration and extraction tool for SCIAMACHY level 1b data by applying all implemented calibration procedures. This includes also the usage of M-factors, which correct for instrumental degradation. These data are the main input for BESD and form the measurement vector with 134 elements in total.

State Vector

BESD retrieves a state vector with 26 elements. It consists of a second order polynomial of the surface spectral albedo in both fit windows, spectral shift and slit functions FWHM in both fit windows, a temperature profile shift, a scaling of the H_2O profile and a default aerosol profile, cloud water/ice path, cloud top height, surface pressure and a ten layered CO_2 mixing ratio profile. Even though the number of state vector elements (26) is smaller than the number of measurement vector elements (134), the inversion problem is generally underdetermined. This especially applies to the ten-layered CO_2 profile. For this reason BESD uses a priori knowledge further constraining the problem and making it well-posed. However, for most of the state vector elements the used a priori knowledge gives only a weak constraint and is therefore not dominating the retrieval results. Furthermore, only static a priori knowledge of XCO_2 is used. The degree of freedom for XCO_2 typically lies within an interval between 0.9 and 1.1

Forward Model

BESD makes use of the SCIATRAN 3.2 radiative transfer code (Rozanov et al., 2005) in discrete ordinate mode. The correlated-k approach of Buchwitz et al. (2000) is used to increase the computational efficiency. As final part of the forward calculation, the resulting spectra are convolved with a SCIAMACHY like Gaussian slit function and applying the dead/bad pixel mask also used for WFM-DOAS 2.1 with additionally masked out all spectral pixels of channel 6+. Spectral line parameters are taken from the HITRAN 2008 (Rothman et al., 2009) database. Pressure, temperature, and humidity profiles are taken from ECMWF.

Inversion Method

BESD uses an optimal estimation based inversion technique to find the most probable atmospheric state given a SCIAMACHY measurement and some prior knowledge. Its quadratic cost function weights the differences between forward model and measurement in respect to the measurement error as well as the difference between retrieved state and a priori knowledge in respect to the a priori uncertainties. A Levenberg-Marquardt method is used to iteratively find the state vector which minimizes the cost function. The Levenberg-Marquardt method has a good-natured convergence behavior because it guarantees that each iteration step actually minimizes the cost function.

Retrieval Output

The result files contain all the information required for surface flux inverse modeling such as retrieved XCO_2 values for individual ground pixels, their errors, corresponding averaging kernels, used a priori profiles, etc. Additionally, the result files contain information about error reduction, information content, degree of freedom, first guess, a priori, and retrieval result of each state vector element as well as the error covariance matrices of the a priori, a posteriori, and the measurement, the gain and averaging kernel matrices, the measurement vector and its spectral fit.

Performance

The validation against ground based FTS measurements and the comparison against CarbonTracker model results show that the algorithm meets the expectations and predictions from earlier theoretical studies. The XCO_2 single measurement precision compared to FTS measurements at the four TCCON sites Park Falls (USA), Bremen (Germany), Darwin (Australia), and Lauder (New Zealand) is 2.5 ppm and similar to theoretical estimates driven by instrumental noise (Reuter et al., 2010). The inferred regional XCO_2 biases between SCIAMACHY and the FTS instruments are in the range of -1.2 ppm (Bremen) and 0.5 ppm (Lauder). All regional biases are smaller than twice their standard error and at two of the four sites they are smaller than their standard error. This means that no statistically significant regional XCO_2 biases are found. BESD produces no significant differences in the year-to-year increase, nor any significant systematic differences in the observed seasonal amplitude when comparing SCIAMACHY XCO_2 with FTS measurements at Park Falls and Darwin.

Computational Speed

BESD requires computational expensive online radiative transfer calculations. One retrieval takes about five minutes on a state of the art single core. Even with strict data pre-filtering, the processing speed is only about four times larger than real time using 24 CPU cores in parallel.

References

Aben, I., Hasekamp, O., and Hartmann, W.: Uncertainties in the space-based measurements of CO_2 columns due to scattering in the Earth's atmosphere, J. Quant. Spectrosc. Radiat. Transfer, 104, 450–459, doi: 10.1016/j.jqsrt.2006.09.013, 2007.

Andrews, A., Boering, K., Daube, B., Wofsy, S., Loewenstein, M., Jost, H., Podolske, J., Webster, C., Herman, R., Scott, D., Flesch, G., Moyer, E., Elkins, J., Dutton, G., Hurst, D., Moore, F., Ray, E., Romashkin, P., and Strahan, S.: Mean ages of stratospheric air derived from in situ observations of CO_2, CH_4, and N_2O, J. Geophys. Res., 106, 32 295–32 314, 2001.

Bösch, H., Toon, G. C., Sen, B., Washenfelder, R. A., Wennberg, P. O., Buchwitz, M., de Beek, R., Burrows, J. P., Crisp, D., Christi, M., Connor, B. J., Natraj, V., and Yung, Y. L.: Space-based near-infrared CO_2 measurements: Testing the Orbiting Carbon Observatory retrieval algorithm and validation concept using SCIAMACHY observations over Park Falls, Wisconsin, J. Geophys. Res., 111, D23302, doi:10.1029/2006JD007080, 2006.

Bovensmann, H., Burrows, J. P., Buchwitz, M., Frerick, J., Noël, S., Rozanov, V. V., Chance, K. V., and Goede, A.: SCIAMACHY – Mission Objectives and Measurement Modes, J. Atmos. Sci., 56, 127–150, 1999.

Bril, A., Oshchepkov, S., Yokota, T., and Inoue, G.: Parameterization of aerosol and cirrus cloud effects on reflected sunlight spectra measured from space: application of the equivalence theorem, Appl. Opt., 46, 2460–2470, 2007.

Buchwitz, M. and Burrows, J. P.: Retrieval of CH_4, CO, and CO_2 total column amounts from SCIAMACHY near-infrared nadir spectra: Retrieval algorithm and first results, in: Remote Sensing of Clouds and the Atmosphere VIII, edited by: Schäfer, K. P., Comèron, A., Carleer, M. R., and Picard, R. H., Proceedings of SPIE, 5235, 375–388, 2004.

Buchwitz, M., Rozanov, V. V., and Burrows, J. P.: A correlated-k distribution scheme for overlapping gases suitable for retrieval of atmospheric constituents from moderate resolution radiance measurements in the visible/near-infrared spectral region, J. Geophys. Res., 105, 15 247–15 261, 2000.

Burrows, J. P., Hölzle, E., Goede, A. P. H., Visser, H., and Fricke, W.: SCIAMACHY – Scanning Imaging Absorption Spectrometer for Atmospheric Chartography, Acta Astronautica, 35, 445–451, 1995.

Butz, A., Hasekamp, O. P., Frankenberg, C., and Aben, I.: Retrievals of atmospheric CO_2 from simulated space-borne measurements of backscattered near-infrared sunlight: accounting for aerosol effects, APPL. OPTICS, 48, 3322–3336, 2009.

Chevallier, F., Bréon, F.-M., and Rayner, P. J.: Contribution of the Orbiting Carbon Observatory to the estimation of CO_2 sources and sinks: Theoretical study in a variational data assimilation framework, J. Geophys. Res., 112, D09307, doi:10.1029/2006JD007375, 2007.

Connor, B. J., Bösch, H., Toon, G., Sen, B., Miller, C., and Crisp, D.: Orbiting carbon observatory: Inverse method and prospective error analysis, J. Geophys. Res.-Atmos., 113, doi:10.1029/2006JD008336, 2008.

Crisp, D., Atlas, R. M., Bréon, F.-M., Brown, L. R., Burrows, J. P., Ciais, P., Connor, B. J., Doney, S. C., Fung, I. Y., Jacob, D. J., Miller, C. E., O'Brien, D., Pawson, S., Randerson, J. T., Rayner, P., Salawitch, R. S., Sander, S. P., Sen, B., Stephens, G. L., Tans, P. P., Toon, G. C., Wennberg, P. O., Wofsy, S. C., Yung, Y. L., Kuang, Z., Chudasama, B., Sprague, G., Weiss, P., Pollock, R., Kenyon, D., and Schroll, S.: The Orbiting Carbon Observatory (OCO) mission, Adv. Space Res., 34, 700–709, 2004.

Deutscher, N. M., Griffith, D. W. T., Bryant, G. W., Wennberg, P. O., Toon, G. C., Washenfelder, R. A., Keppel-Aleks, G., Wunch, D., Yavin, Y., Allen, N. T., Blavier, J.-F., Jiménez, R., Daube, B. C., Bright, A. V., Matross, D. M., Wofsy, S. C., and Park, S.: Total column CO_2 measurements at Darwin, Australia - site description and calibration against in situ aircraft profiles, Atmos. Meas. Tech., 3, 947–958, doi:10.5194/amt-3-947-2010, URL http://www.atmos-meas-tech.net/3/947/2010/, 2010.

Efron, B.: Bootstrap Methods - Another Look at the Jackknife, Annals of Statistics, 7, 1–26, 1979.

Houweling, S., Breon, F.-M., Aben, I., Rödenbeck, C., Gloor, M., Heimann, M., and Ciais, P.: Inverse modeling of CO_2 sources and sinks using satellite data: a synthetic inter-comparison of measurement techniques and their performance as a function of space and time, Atmos. Chem. Phys., 4, 523–538, 2004.

Houweling, S., Hartmann, W., Aben, I., Schrijver, H., Skidmore, J., Roelofs, G.-J., and Breon, F.-M.: Evidence of systematic errors in SCIAMACHY-observed CO_2 due to aerosols, Atmos. Chem. Phys., 5, 3003–3013, 2005.

King, J.: Validation of ECMWF sea level pressure analyses over the Bellingshausen Sea, Antarctica, Weather Forecast, 18, 536–540, 2003.

Kuang, Z., Margolis, J., Toon, G., Crisp, D., and Yung, Y.: Spaceborne measurements of atmospheric CO_2 by high-resolution NIR spectrometry of reflected sunlight: an introductory study, Geophy. Res. Let., 29, 1716, doi: 10.1029/2001GL014298, 2002.

Lammert, A., Bruemmer, B., Ebbers, I., and Mueller, G.: Validation of ECMWF and DWD model analyses with buoy measurements over the Norwegian Sea, Meteorol. Atmos. Phys., 102, 87–96, doi:10.1007/s00703-008-0008-1, 2008.

Messerschmidt, J., Macatangay, R., Notholt, J., Petri, C., Warneke, T., and Weinzierl, C.: Side by side measurements of CO_2 by ground-based Fourier transform spectrometry (FTS), Tellus B, doi:10.1111/j.1600-0889.2010.00491.x, 2010.

Miller, C. E., Crisp, D., DeCola, P. L., Olsen, S. C., Randerson, J. T., Michalak, A. M., Alkhaled, A., Rayner, P., Jacob, D. J., Suntharalingam, P., Jones, D. B. A., Denning, A. S., Nicholls, M. E., Doney, S. C., Pawson, S., Bösch, H., Connor, B. J., Fung, I. Y., O'Brien, D., Salawitch, R. J., Sander, S. P., Sen, B., Tans, P., Toon, G. C., Wennberg, P. O., Wofsy, S. C., Yung, Y. L., and Law, R. M.: Precision requirements for space-based X_{CO_2} data, J. Geophys. Res., 112, D10314, doi:10.1029/2006JD007659, 2007.

Nakajima, T. and King, M. D.: Determination of optical thickness and effective particle radius of clouds from reflected solar radiation measurements. Part I: Theory, J. Atmos. Sci., 47, 1878–1893, 1990.

Peters, W., Jacobson, A. R., Sweeney, C., Andrews, A. E., Conway, T. J., Masarie, K., Miller, J. B., Bruhwiler, L. M. P., Pétron, G., Hirsch, A. I., Worthy, D. E. J., van der Werf, G. R., Randerson, J. T., Wennberg, P. O., Krol, M. C., and Tans, P. P.: An atmospheric perspective on North American carbon dioxide exchange: CarbonTracker, Proceedings of the National Academy of Sciences (PNAS) of the United States of America, November 27, 2007, 104, 18 925–18 930, 2007.

Rayner, P. J. and O'Brien, D. M.: The utility of remotely sensed CO_2 concentration data in surface inversions, Geophys. Res. Lett., 28, 175–178, 2001.

Reuter, M., Buchwitz, M., Schneising, O., Heymann, J., Bovensmann, H., and Burrows, J. P.: A method for improved SCIAMACHY CO_2 retrieval in the presence of optically thin clouds, Atmos. Meas. Tech., 3, 209–232, URL http://www.atmos-meas-tech.net/3/209/2010/, 2010.

Reuter, M., Bovensmann, H., Buchwitz, M., Burrows, J. P. Connor, B. J., Deutscher, N. M., Griffith, D. W. T., Heymann, J., Keppel-Aleks, G., Messerschmidt, J., Notholt, J., Petri, C., Robinson, J., Schneising, O., Sherlock, V., Velazco, V., Warneke, T., Wennberg, P. O., and Wunch, D.: Retrieval of atmospheric CO_2 with enhanced accuracy and precision from SCIAMACHY: Validation with FTS measurements and comparison with model results., J. Geophys. Res., 116, 2011.

Rodgers, C. D.: Inverse Methods for Atmospheric Sounding: Theory and Practice, World Scientific Publishing, 2000.

Rothman, L. S., Gordon, I. E., Barbe, A., Benner, D. C., Bernath, P. E., Birk, M., Boudon, V., Brown, L. R., Campargue, A., Champion, J. P., Chance, K., Coudert, L. H., Dana, V., Devi, V. M., Fally, S., Flaud, J. M., Gamache, R. R., Goldman, A., Jacquemart, D., Kleiner, I., Lacome, N., Lafferty, W. J., Mandin, J. Y., Massie, S. T., Mikhailenko, S. N., Miller, C. E., Moazzen-Ahmadi, N., Naumenko, O. V., Nikitin, A. V., Orphal, J., Perevalov, V. I., Perrin, A., Predoi-Cross, A., Rinsland, C. P., Rotger, M., Simeckova, M., Smith, M. A. H., Sung, K., Tashkun, S. A., Tennyson, J., Toth, R. A., Vandaele, A. C., and Vander Auwera, J.: The HITRAN 2008 molecular spectroscopic database, J. Quant. Spectrosc. Ra., 110, 533–572, doi:10.1016/j.jqsrt.2009.02.013, 2009.

Rozanov, A., Rozanov, V., Buchwitz, M., Kokhanovsky, A., and Burrows, J.: SCIATRAN 2.0 - A new radiative transfer model for geophysical applications in the 175-2400 nm spectral region, in: Atmospheric remote sensing: Earth's surface, troposphere, stratosphere and mesosphere - I, edited by Burrows, JP and Eichmann, KU, vol. 36 of *Adv. Space Res.*, pp. 1015–1019, doi: 10.1016/j.asr.2005.03.012, 35th COSPAR Scientific Assembly, Paris, France, JUL 18-25, 2004, 2005.

Schneising, O., Buchwitz, M., Burrows, J. P., Bovensmann, H., Reuter, M., Notholt, J., Macatangay, R., and Warneke, T.: Three years of greenhouse

gas column-averaged dry air mole fractions retrieved from satellite - Part 1: Carbon dioxide, Atmos. Chem. Phys., 8, 3827–3853, 2008.

Stephens, B. B., Gurney, K. R., Tans, P. P., Sweeney, C., Peters, W., Bruhwiler, L., Ciais, P., Ramonet, M., Bousquet, P., Nakazawa, T., Aoki, S., Machida, T., Inoue, G., Vinnichenko, N., Lloyd, J., Jordan, A., Heimann, M., Shibistova, O., Langenfelds, R. L., Steele, L. P., Francey, R. J., and Denning, A. S.: Weak northern and strong tropical land carbon uptake from vertical profiles of atmospheric CO_2, Science, 316, 1732–1735, doi:10.1126/science.1137004, 2007.

Tolk, L. F., Meesters, A. G. C. A., Dolman, A. J., and Peters, W.: Modelling representation errors of atmospheric CO_2 mixing ratios at a regional scale, Atmos. Chem. Phys., 8, 6587–6596, 2008.

Washenfelder, R. A., Toon, G. C., Blavier, J.-F., Yang, Z., Allen, N. T., Wennberg, P. O., Vay, S. A., Matross, D. M., and Daube, B. C.: Carbon dioxide column abundances at the Wisconsin Tall Tower site, J. Geophys. Res., 111, D22305, doi:10.1029/2006JD007154, 2006.

Wunch, D., Toon, G. C., Wennberg, P. O., Wofsy, S. C., Stephens, B. B., Fischer, M. L., Uchino, O., Abshire, J. B., Bernath, P., Biraud, S. C., Blavier, J.-F. L., Boone, C., Bowman, K. P., Browell, E. V., Campos, T., Connor, B. J., Daube, B. C., Deutscher, N. M., Diao, M., Elkins, J. W., Gerbig, C., Gottlieb, E., Griffith, D. W. T., Hurst, D. F., Jiménez, R., Keppel-Aleks, G., Kort, E. A., Macatangay, R., Machida, T., Matsueda, H., Moore, F., Morino, I., Park, S., Robinson, J., Roehl, C. M., Sawa, Y., Sherlock, V., Sweeney, C., Tanaka, T., and Zondlo, M. A.: Calibration of the Total Carbon Column Observing Network using aircraft profile data, Atmos. Meas. Tech., 3, 1351–1362, doi:10.5194/amt-3-1351-2010, URL http://www.atmos-meas-tech.net/3/1351/2010/, 2010.

Wunch, D., Wennberg, P. O., Toon, G. C., Connor, B. J., Fisher, B., Osterman, G. B., Frankenberg, C., Mandrake, L., O'Dell, C., Ahonen, P., Biraud, S. C., Castano, R., Cressie, N., Crisp, D., Deutscher, N. M., Eldering, A., Fisher, M. L., Griffith, D. W. T., Gunson, M., Heikkinen, P., Keppel-Aleks, G., Kyrö, E., Lindenmaier, R., Macatangay, R., Mendonca, J., Messerschmidt, J., Miller, C. E., Morino, I., Notholt, J., Oyafuso, F. A., Rettinger, M., Robinson, J., Roehl, C. M., Salawitch, R. J., Sherlock, V., Strong, K., Sussmann, R., Tanaka, T., Thompson, D. R., Uchino, O., Warneke, T., and Wofsy, S. C.: A method for evaluating bias in

global measurements of CO_2 total columns from space, Atmospheric Chemistry and Physics, 11, 12 317–12 337, doi:10.5194/acp-11-12317-2011, URL http://www.atmos-chem-phys.net/11/12317/2011/, 2011.

Yokota, T., Oguma, H., Morino, I., and Inoue, G.: A nadir looking SWIR sensor to monitor CO_2 column density for Japanese GOSAT project, Proceedings of the twenty-fourth international symposium on space technology and science. Miyazaki: Japan Society for Aeronautical and Space Sciences and ISTS, pp. 887–889, 2004.